

2022-06-17

Plasma Imaging, Local Measurement, and Tomographic experiment (PILOT): a mission concept for transformational multi-scale observations of mass and energy flow dynamics in Earth's magnetosphere

D. Malaspina, R. Ergun, J. Goldstein, C. Spittler, L. Andersson, J. Borovsky, X. Chu, L. De Moudt, D. Gallagher, V. Jordanova, S. Lejosne, J. Link, N. Maruyama, J. Parker, S. Thaller, B. Unruh, B. Walsh. 2022. "Plasma Imaging, Local Measurement, and Tomographic Experiment (PILOT): A Mission Concept for Transformational Multi-Scale Observations of Mass and Energy Flow Dynamics in Earth's Magnetosphere" *Frontiers in Astronomy and Space Sciences*, Volume 9. <https://doi.org/10.3389/fspas.2022.910730>

<https://hdl.handle.net/2144/46007>

"Downloaded from OpenBU. Boston University's institutional repository."



Plasma Imaging, LOcal Measurement, and Tomographic Experiment (PILOT): A Mission Concept for Transformational Multi-Scale Observations of Mass and Energy Flow Dynamics in Earth's Magnetosphere

OPEN ACCESS

Edited by:

Luca Sorriso-Valvo,
Institute for Space Physics (Uppsala),
Sweden

Reviewed by:

Filomena Catapano,
European Space Research Institute
(ESRIN), Italy
Rungployphan Om Kieokaew,
UMR5277 Institut de Recherche en
Astrophysique et Planétologie (IRAP),
France

*Correspondence:

David Malaspina
David.Malaspina@colorado.edu

Specialty section:

This article was submitted to
Space Physics,
a section of the journal
Frontiers in Astronomy and Space
Sciences

Received: 01 April 2022

Accepted: 17 May 2022

Published: 17 June 2022

Citation:

Malaspina D, Ergun R, Goldstein J, Spittler C, Andersson L, Borovsky J, Chu X, De Moudt L, Gallagher D, Jordanova V, Lejosne S, Link J, Maruyama N, Parker J, Thaller S, Unruh B and Walsh B (2022) Plasma Imaging, LOcal Measurement, and Tomographic Experiment (PILOT): A Mission Concept for Transformational Multi-Scale Observations of Mass and Energy Flow Dynamics in Earth's Magnetosphere. *Front. Astron. Space Sci.* 9:910730. doi: 10.3389/fspas.2022.910730

David Malaspina^{1,2*}, Robert Ergun^{1,2}, Jerry Goldstein³, Constance Spittler², Laila Andersson², Joseph Borovsky⁴, Xiangning Chu², Lauren De Moudt⁵, Dennis Gallagher⁶, Vania Jordanova⁷, Solène Lejosne⁸, Jason Link², Naomi Maruyama², Jeffery Parker⁵, Scott Thaller², Bryce Unruh² and Brian Walsh⁹

¹Astrophysical and Planetary Sciences Department, University of Colorado, Boulder, CO, United States, ²Laboratory for Atmospheric and Space Physics, University of Colorado, Boulder, CO, United States, ³Southwest Research Institute, San Antonio, TX, United States, ⁴Space Science Research Institute, Boulder, CO, United States, ⁵Advanced Space LLC, Westminster, CO, United States, ⁶NASA Marshall Spaceflight Research Center, Huntsville, AL, United States, ⁷Los Alamos National Laboratory, Los Alamos, NM, United States, ⁸Space Sciences Laboratory, University of California, Berkeley, Berkeley, CA, United States, ⁹College of Engineering, Boston University, Boston, MA, United States

We currently do not understand the fundamental physical processes that govern mass and energy flow through the Earth's magnetosphere. Knowledge of these processes is critical to understanding the mass loss rate of Earth's atmosphere, as well as for determining the role that a planetary magnetic field plays in atmospheric retention, and therefore habitability, for Earth-like planets beyond the solar system. Mass and energy flow processes are challenging to determine at Earth in part because Earth's planetary magnetic field creates a complex "system of systems" composed of interdependent plasma populations and overlapping spatial regions that perpetually exchange mass and energy across a broad range of temporal and spatial scales. Further, the primary mass carrier in the magnetosphere is cold plasma (as cold as ~0.1 eV), which is invisible to many space-borne instruments that operate in the inner magnetosphere. The Plasma Imaging LOcal and Tomographic experiment (PILOT) mission concept, described here, provides the transformational multi-scale observations required to answer fundamental open questions about mass and energy flow dynamics in the Earth's magnetosphere. PILOT uses a constellation of spacecraft to make radio tomographic, remote sensing, and *in-situ* measurements simultaneously, fully capturing cold plasma mass dynamics and its impact on magnetospheric systems over an unprecedented range of spatial and temporal scales. This article details the scientific motivation for the PILOT mission concept as well as a potential mission implementation.

Keywords: inner magnetosphere, plasmasphere, cold plasma, mission concept, mass transport

1 INTRODUCTION

Magnetospheric physics has a massive problem: we have not yet determined the fundamental processes that govern plasma mass and energy flow through the terrestrial magnetosphere, nor the degree to which these flows regulate key magnetospheric subsystems.

Hundreds of metric tons of ionized atmospheric gases pass into and through Earth's magnetic field. This mass accumulates in inner magnetospheric reservoirs, is transported through the magnetosphere, where it profoundly regulates magnetospheric subsystems, and can eventually be lost to the solar wind. Cold plasma ($< 1\text{--}100\text{ eV}$) carries the overwhelming majority of this mass, and tracking its flow is the weakest link in our chain of understanding for magnetospheric physics (Delzanno et al., 2021). Currently, we understand more about the physics of atmospheric mass loss at Mars and Venus than we do at Earth (Titov et al., 2006; Jakosky, 2015). Understanding magnetospheric mass flows and associated energy flows is critical to understanding the mass loss rate of Earth's atmosphere, as well as to determining the importance of a planetary magnetic field for atmospheric retention (Ramstad and Barabash, 2021), and therefore habitability, for Earth-like planets beyond the solar system.

Knowledge gaps related to the processes that govern plasma mass and energy flow through the magnetosphere have persisted through decades of magnetospheric measurements due to three primary limitations. First, the Earth's planetary magnetic field creates a complex "system of systems" composed of interdependent plasma populations and overlapping spatial regions that perpetually exchange mass and energy. Because of this complexity, inherent to any planet with an internal dynamo-driven magnetic field, measurements are required that span a broad range of temporal and spatial scales in order to disentangle the coupled processes that drive mass and energy flow. Second, cold plasma is not directly detectable by most space-borne particle instruments traversing the inner magnetosphere, because its thermal energy is well below the floating electrical potential of spacecraft surfaces immersed in the ambient plasma (Delzanno et al., 2021). To make new progress, instrumentation specifically designed to detect cold plasma is required. Third, prior observations of mass flow and its impact on magnetospheric subsystems are limited to either single-spacecraft local measurements of total plasma density with limited composition data and no contextual mass spatial distribution information (Engwall et al., 2009; Kurth et al., 2015; Andriopoulou et al., 2018), or to single-view line-of-sight integrated measurements of minor ion species without *in-situ* measurements embedded in the imaged plasma (Sandel et al., 2001). New progress requires combining measurements of the plasma mass spatial distribution in the inner magnetosphere with simultaneous embedded *in-situ* measurements.

The Plasma Imaging LOcal and Tomographic experiment (PILOT) mission concept overcomes all three of these limitations by using a constellation of 34 spacecraft to simultaneously make rapidly refreshing, spatially resolved images of total plasma density in the equatorial plane, images

of ion density and flows in the meridional plane, and *in-situ* ground-truth measurements embedded within the imaged regions.

The PILOT mission concept constellation consists of 30 identical microsat spacecraft ("RadioSats") and four smallsat spacecraft ("PlasmaSats") in two near-equatorial orbits. The network of RadioSats produce equatorial plasma density images through radio tomographic inversion of a network of line-of-sight total electron content (TEC) measurements (see **Supplementary Appendix S1** and Ergun et al. (2000)), combined with *in-situ* total plasma density measurements. The resulting density images have high spatial ($\sim 0.5 R_E$) and temporal ($\sim 15\text{ s}$) resolution. Meridional ion density and flows are determined by imaging extreme ultraviolet (EUV) photons at 30.4 nm (He^+) and 83.4 nm (O^+/O^{++}) (Sandel et al., 2001; Burch et al., 2001a; Burch et al., 2001b; Burch, 2001; Goldstein et al., 2003; Goldstein et al., 2018; Goldstein et al., 2019), with high spatial ($\sim 0.05 R_E$) and temporal ($< 15\text{ s}$) resolution. Two of the four PlasmaSats carry EUV instruments. All four PlasmaSats are equipped to make embedded *in-situ* measurements of both DC-coupled and AC-coupled electric and magnetic fields, cold plasma composition, flux, and distribution functions, as well as energetic proton and electron flux and distribution functions.

The PILOT spacecraft are arranged in two highly-elliptical orbits ($1.52 R_E \times 4.25 R_E$ and $1.10 R_E \times 6.25 R_E$). The orbits are optimized to enable 1) near-equatorial radio tomographic images with instantaneous coverage over a large region of the inner magnetosphere: ~ 3 Earth radii (R_E) in radial distance and ~ 3 hrs in MLT, 2) coverage in the meridional plane of $\pm 4.8 R_E$ for He^+ images and $\pm 2.2 R_E$ for O^+ images, and 3) *in-situ* measurements along orbits with apogees near L-shells of 4 and 6, embedded within the imaged plasma.

The PILOT implementation leverages several technological innovations to support a fully feasible mission. First, spacecraft manufacturing has matured to the point where numerous commercial vendors exist that can produce spacecraft in the quantities needed for radio tomographic imaging (a few tens of spacecraft). Second, instrumentation miniaturization has progressed such that relatively small spacecraft can host the range of instruments needed for PILOT *in-situ* measurements. Third, the launch and deployment of large spacecraft constellations has become commonplace, and a number of technologies that enable constellation deployment are now available.

By taking advantage of these technological advancements, the PILOT mission concept makes the transformational measurements needed to close fundamental and persistent knowledge gaps about mass and energy flow through the magnetosphere of a magnetized terrestrial planet.

The following sections first lay out the specific science goals and objectives that motivate the PILOT mission concept, then discuss the measurements required to achieve them. A mission implementation is then described, including notional orbits, spacecraft bus configurations, and instrumentation. A detailed discussion on the generation of plasma density images by radio tomography for PILOT is included in **Supplementary Appendix S1**. Finally, inversion and forward model algorithms that can be

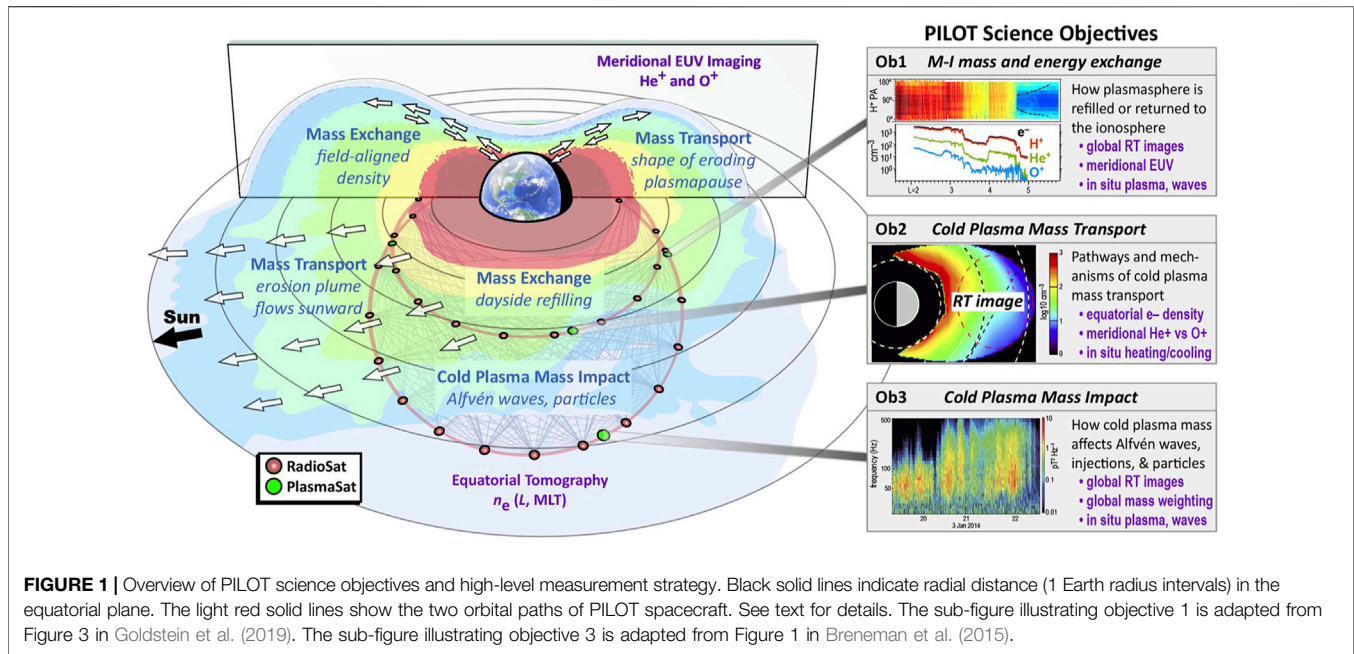


FIGURE 1 | Overview of PILOT science objectives and high-level measurement strategy. Black solid lines indicate radial distance (1 Earth radius intervals) in the equatorial plane. The light red solid lines show the two orbital paths of PILOT spacecraft. See text for details. The sub-figure illustrating objective 1 is adapted from Figure 3 in Goldstein et al. (2019). The sub-figure illustrating objective 3 is adapted from Figure 1 in Breneman et al. (2015).

used for EUV image deconvolution are discussed in **Supplementary Appendix S2**.

2 MOTIVATING SCIENCE GOALS AND OBJECTIVES

The driving science goal of PILOT is to determine the primary pathways of mass and energy flow through the coupled systems of the terrestrial magnetosphere. This goal motivates three specific science objectives. Each targets a critical aspect of mass and energy exchange among the plasma populations that make up the magnetospheric meta-system. The science objectives are arranged to “follow the mass” as ionized gases exit the ionosphere, enter and are transported through and out of the inner magnetosphere, and profoundly modify magnetospheric systems and magnetospheric energy transport along their journey.

The PILOT science objectives are: 1) Identify and quantify the key processes that govern mass and energy exchange between the ionosphere and the magnetosphere, 2) Discover the pathways and processes governing cold plasma mass transport through and out of the inner magnetosphere, and 3) Determine how, where, and when cold plasma mass acts most efficiently to regulate coupling between magnetospheric regions and between plasma populations. Achieving each science objective requires addressing specific science questions, listed and described below.

Figure 1 presents an overview of PILOT’s science objectives and high-level measurement strategy: simultaneous radio tomography, EUV imaging, and embedded *in-situ* measurement. The radio tomographic mesh formed by the RadioSats is shown in the equatorial plane, the meridional plane imaged by the outer-orbit PlasmaSatEUV instruments is

shown, and locations of all four *in-situ* measurements (PlasmaSats) are indicated. RadioSats and PlasmaSats are discussed in **Section 3.1**. Plasma density is represented by colored contours, where the equatorial mass distribution is adapted from an EUV image in Figure 2B of Goldstein et al. (2004a). The meridional mass distribution is schematic, based on simulated EUV images created using the forward model of Goldstein et al. (2018). PILOT’s three science objectives (Ob1, Ob2, and Ob3) are indicated on the right of the figure. The science questions that underpin those objectives are discussed in detail next.

2.1 Objective 1, Science Question 1a: How Is the Plasmasphere Refilled From Ionospheric Sources?

When atmospheric gases are ionized, by solar radiation or electron bombardment, electromagnetic interaction with the solar wind causes them to flow out of the ionosphere (e.g., Banks, 1968; Banks, 1969; Singh and Horwitz, 1992). Earth’s planetary magnetic field traps much of this plasma in the plasmasphere, preventing it from escaping directly to the solar wind (Chappell, 2015). During geomagnetic storms, some of the mass held in this reservoir is forced into the solar wind and lost from the magnetosphere. Ionospheric outflow then refills the plasmaspheric reservoir and the process repeats (Hultqvist et al., 1999; Welling et al., 2015).

After decades of research, fundamental questions concerning plasmaspheric refilling remain unanswered. The observations required to address these questions do not yet exist (Gallagher et al., 2021). In this observational void, gaps in our basic knowledge persist: What causes refilling rates to vary by orders of magnitude? Why is the amount of mass trapped by the magnetosphere only weakly correlated with the polar

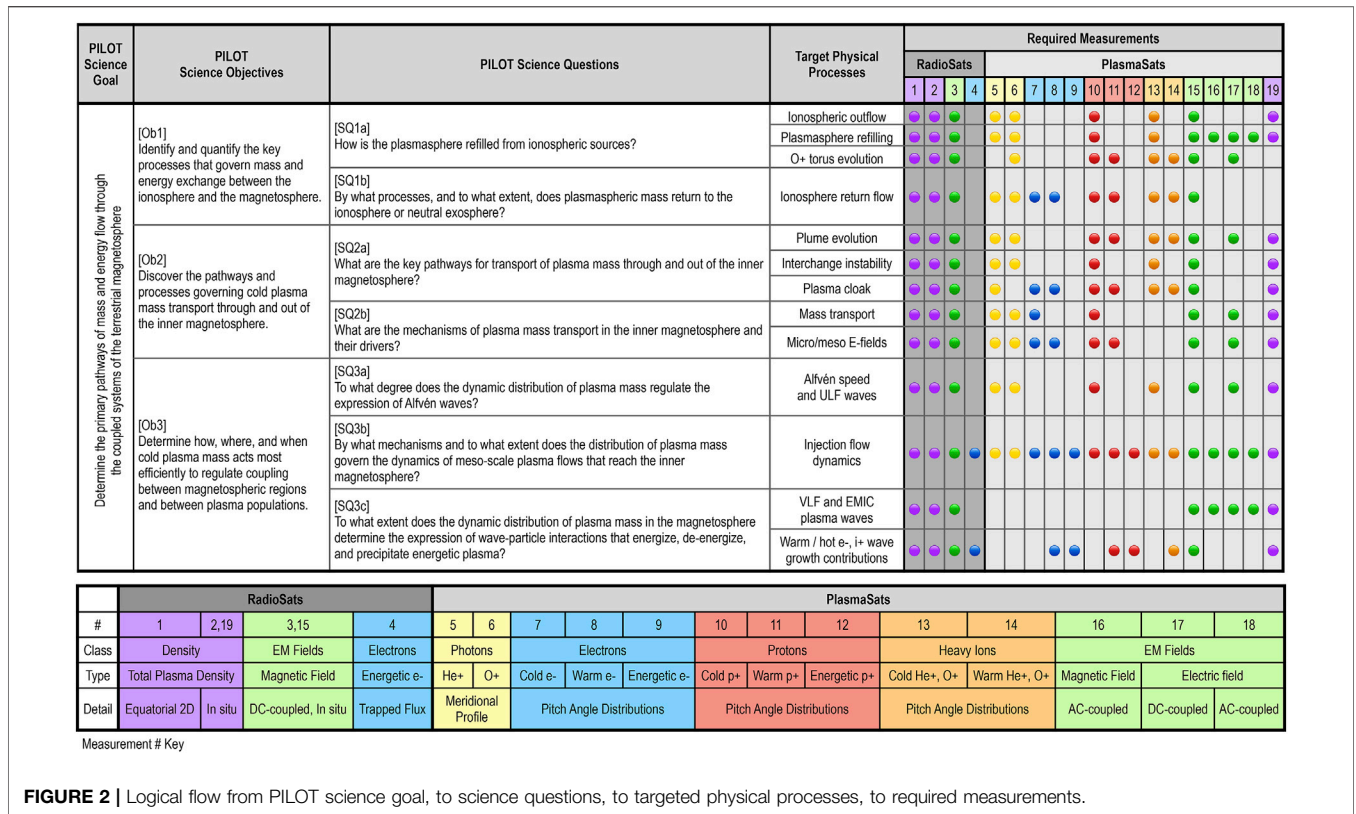


FIGURE 2 | Logical flow from PILOT science goal, to science questions, to targeted physical processes, to required measurements.

outflow rates (Denton et al., 2012)? What fundamental plasma processes are responsible for trapping new ions in the plasmasphere torus (Goldstein et al., 2020; Goldstein et al., 2021)?

Ionospheric outflow and plasmaspheric refilling shows intense variability (Gallagher et al., 2021). For $2.5 \leq L \leq 4.5$ refilling rates range from 4 to $800 \text{ cm}^{-3} \text{ day}^{-1}$ (Park, 1973; Park, 1974; Farrugia et al., 1989; Carpenter et al., 1993; Reinisch et al., 2004; Dent et al., 2006; Sandel and Denton, 2007; Gallagher et al., 2021). At geosynchronous orbit, quiet-time refilling rates range from as little as $\sim 0.6 \text{ cm}^{-3} \text{ day}^{-1}$ (Lawrence et al., 1999) to as much as $50 \text{ cm}^{-3} \text{ day}^{-1}$ (Sojka et al., 1986). In stark contrast, Borovsky et al. (2014) discovered long-lived plasmaspheric plume active-time events at geosynchronous orbit that could only persist if fueled by refilling rates of $100\text{--}500 \text{ cm}^{-3} \text{ day}^{-1}$.

We lack basic knowledge about the formation of the dense O^+ torus in the outer plasmasphere (Horwitz and Lockwood, 1985; Roberts et al., 1987; Andersson et al., 2005; Goldstein et al., 2018; Hull et al., 2019). Two possible origins for the O^+ torus have been identified: it may originate from the local ionosphere near the magnetic equator, or it could arrive in part or in total from high latitude as the low energy portion of the warm plasma cloak (Chappell et al., 2008).

The PILOT mission concept achieves closure on this science question by comparing multi-scale measurements of cold plasma mass flow and variability over a broad swath of the inner magnetosphere against theories for ion trapping (Hrbáčková et al., 2015), refilling variability (Gallagher et al., 2021),

refilling mass dependence (Sandel, 2011), and O^+ torus formation (Goldstein et al., 2018).

These comparisons are enabled by direct and simultaneous measurement of: 1) spatially and temporally resolved plasma density across a broad region of the near-equatorial inner magnetosphere [$\geq 3 \text{ h}$ Magnetic Local Time (MLT)], covering radial distances ($3 < L\text{-shell} < 6$) where field aligned ions are converted into trapped isotropic distributions during plasmasphere refilling, 2) global meridional EUV-He measurements to quantify the spatial and temporal evolution of field-aligned light ion distributions, 3) *in-situ* observations, embedded within the imaged regions, of cold ($0.1\text{--}100 \text{ eV}$) H^+ , He^+ , and O^+ distribution functions, densities, and temperatures, as well as plasma waves that may isotropize outflowing ions (Gurnett, 1976; Olsen et al., 1987; Boardsen et al., 1992; Singh, 1996; Hrbáčková et al., 2015), and 4) EUV global meridional imaging of O^+ , to determine the extent to which O^+ torus ions are supplied from the ionosphere, by cusp outflow, or directly from the auroral zone (Horwitz and Lockwood, 1985; Roberts et al., 1987; Hull et al., 2019). Imaging the O^+ torus enables its basic morphology to be quantified, including its symmetry (or lack thereof) in MLT, its latitudinal extent, and what processes control these attributes (Nosé et al., 2011; Nosé et al., 2015; Goldstein et al., 2018; Nosé et al., 2018). *In-situ* observations for this science question must cover radial distances where refilling is most dynamic ($3 < L\text{-shell} < 6$), in the minutes, hours, and days that follow geomagnetically active times.

2.2 Objective 1, Science Question 1b: By What Processes, and to What Extent, Does Plasmaspheric Mass Return to the Ionosphere or Neutral Exosphere?

A full accounting of mass flow between the ionosphere and plasmasphere must include flow from the plasmasphere back into the ionosphere (Lemaire and Gringauz, 1998) or neutral exosphere (Nass and Fahr, 1984). There is a large knowledge gap related to this mass flow pathway. In the absence of sunlight, low-altitude recombination reduces ion pressure gradients, which is expected to cause downward transport (Lemaire and Gringauz, 1998; Gallagher et al., 2021), allowing nightside flux tubes to return plasmaspheric mass to the ionosphere. This mechanism may explain the anomalous mass loss reported on L-shells far from the eroded plasmopause boundary (Gallagher et al., 2021). However, the cross-scale measurements required to test this hypothesis, or to identify a new one, currently do not exist.

PILOT achieves closure on this science question by comparing existing predictions for downward ion transport of plasmaspheric mass (Gallagher et al., 2021) with direct multi-scale measurements of cold plasma mass content and its variability.

Making these comparisons requires direct and simultaneous measurements of: 1) spatially and temporally resolved total plasma density over several hours of MLT and several L-shell, 2) meridional imaging of ionospheric plasma inflows (of both light ions and O^+), and 3) *in-situ* observations of cold (0.1–100 eV) proton and heavy ion distribution functions embedded in the imaged regions. The observations most effective at addressing this science question will be within $3 < L\text{-shell} < 5$, where plasmopause erosion is weakly active during quiet or moderately-disturbed times.

2.3 Objective 2, Science Question 2a: What Are the Key Pathways for Transport of Plasma Mass Through and Out of the Inner Magnetosphere?

After cold plasma mass reaches the plasmasphere, it is distributed and transported to other magnetospheric regions. Known and speculated mass transport pathways include plasmaspheric plume flows (Darrouzet et al., 2009), interchange instability (Pierrard and Lemaire, 2004), and the warm plasma cloak (Borovsky et al., 2013; Gallagher and Comfort, 2016). Each transport pathway is driven by different, sometimes competing, physical mechanisms. Limited existing measurements prevent us from knowing which mass flow pathways are most important under which geomagnetic conditions, what feedback exists among transport mechanisms, and how these mechanisms combine to produce the observed distribution of mass in the magnetosphere.

A plasmaspheric plume is a dramatic structure formed by sunward plasma transport, where the density can be 50–100 times greater than adjacent regions. A plume can span many Earth radii ($5 R_E$ or more) or be narrow ($< 1 R_E$). A plume can detach from the plasmasphere and extend into the dayside magnetopause. A basic understanding of how a plasmaspheric plume forms and

maintains itself is lacking. A plume can form over the course of tens of minutes. It can be short lived (hours) or last for weeks (Borovsky et al., 2014; Krall et al., 2018). The physics that drives the refilling necessary to sustain this structure and quantification of the appropriate refilling rates both remain poorly determined (Denton and Borovsky, 2014; Gallagher and Comfort, 2016).

The warm plasma cloak is a population outside the plasmasphere transported in from the magnetotail, rich with oxygen (Chappell et al., 2008; Nose et al., 2015; Jahn et al., 2017). Many key questions remain about the transport and coupling of this population. What mechanism is responsible for heating the cloak plasma (Hill et al., 2020)? Does the plasma cloak play a dominant role in mass loading the dayside magnetosphere (Borovsky et al., 2013)? Is the cloak a candidate for nightside plasmasphere refilling (Gallagher and Comfort, 2016)?

PILOT achieves closure on this science question by comparing the observed morphology of cold plasma flows in the near-equatorial magnetosphere, and signatures of cold ion heating or cooling, against theoretical expectations for each pathway.

These comparisons require measurement of rapidly refreshing images of total plasma density in the near-equatorial plane across several MLT in the inner magnetosphere. Observations must target radial distances where strong transport is observed ($3 < L < 6$). Simultaneously, meridional plasma flows of He^+ and O^+ must be imaged to determine whether equatorial plasma density changes are due to flows out of the equatorial plane or within it. Embedded *in-situ* observations of heavy (He^+ , O^+) and light (H^+) ion distributions spanning 0.1–100 eV are required to observe heating or cooling of cold plasma that may be a prerequisite for some transport pathways (Borovsky et al., 2013).

2.4 Objective 2, Science Question 2b: What Are the Mechanisms of Plasma Mass Transport and Their Drivers?

Once ionospheric plasma mass reaches the plasmasphere, it may go sunward to the dayside magnetopause and participate in reconnection, or it may be diverted to the flanks and travel anti-sunward to load the plasmashet. What fundamental mechanisms dictate the transport and distribution of this mass?

Mass transport is expected to be primarily determined by the dynamic electric and magnetic fields in the magnetosphere. While the geomagnetic field is relatively well-known, the electric (E) field is more elusive. Single-point *in-situ* E-field measurements have been leveraged to create empirical models, i.e., statistical maps. However, empirical models usually impose an electrostatic assumption ($\nabla \times E = 0$). Although it facilitates visualization of convective pathways (Matsui et al., 2013), the validity of this assumption is questionable, in particular at higher L-shells. It is also difficult to quantify the extent to which statistical models can accurately describe dynamical evolution in case studies.

Moreover, statistical data analysis blurs/obscures small scale features and/or highly structured features naturally present in the database. These features include sub-auroral polarization streams (SAPS) (Foster et al., 2007) and sub-auroral ion drifts (SAID) (Anderson et al., 1991). While statistical experimental models for

SAPS exist (Kunduri et al., 2018), how they connect to the global topology of the electric fields, thus, how they organize plasma mass transport, remains unclear (Elphic et al., 1997; Liemohn et al., 2004; Foster et al., 2020).

Small-scale features are definitely present in the global electric field topology, but their role in plasma transport remains to be determined. For instance, to what extent is plasmasphere erosion governed by global vs. local electric field dynamics? Observations from the IMAGE EUV instrument revealed the existence of many small scale structures on the plasmasphere boundary, including notches, crenulations, fingers and shoulders. The time evolution of these structures was leveraged to extract information about the average spatial variability of the large-scale DC electric field (Galvan et al., 2010). Yet statistical models for the electric field dynamics seldom accurately reproduce such features (Goldstein and Sandel, 2005).

PILOT achieves closure on this science question by comparing electric field drivers and magnetic field context with the resulting plasma mass motion, allowing key transport mechanisms to be identified.

Measuring bulk plasma motion requires rapidly refreshing images of total density in the equatorial plane. Embedded in the image plane, *in-situ* point observations of DC-coupled electric and magnetic fields, along with measurements of cold proton, electron, and heavy ion distribution functions, provide ground truth point-sampling of the cold plasma bulk motion and the electric fields that drive it. Simultaneous meridional imaging of cold plasma flow is required to quantify transport into and out of the equatorial plane. This set of measurements enables determination of the mechanisms and drivers of cold plasma mass transport.

2.5 Objective 3, Science Question 3a: To What Degree Does the Dynamic Distribution of Plasma Mass Regulate the Expression of Alfvén Waves?

Propagating at the Alfvén speed, Ultra Low Frequency (ULF) waves carry information via magnetic field fluctuations that enable magnetosphere-ionosphere coupling (Lysak, 1990), magnetosphere-solar wind coupling (Wright, 1996), as well as radiation belt energization and particle transport via radial diffusion (Elkington et al., 2003).

The inner magnetosphere supports various ULF modes, including those that carry energy Earthward from the magnetotail and from the magnetopause (Takahashi et al., 2015). These energy inputs can either drive propagating waves, or drive field line resonances and cavity modes (Dungey, 1955; Samson and Rostoker, 1972; Kivelson and Southwood, 1985; Lee and Lysak, 1989; Samson et al., 1992). Energy flux transport *via* these modes, and energy exchange between these modes is critically sensitive to the Alfvén speed.

Modeling has shown that the spatial distribution of plasma mass should significantly alter the ULF wave power distribution, both radially and in MLT. For example, the plasma mass distribution determines the radial location where the compressional (fast mode) radial wavenumber goes to zero,

beyond which compressional waves transfer energy into local field line resonances (Claudepierre et al., 2016).

PILOT achieves closure on this science question by measuring the dynamic spatial distribution of Alfvén speed, across scale sizes, over a broad region of the inner magnetosphere, while simultaneously quantifying the degree to which this distribution regulates ULF plasma wave properties.

Determining the spatial distribution of Alfvén speed requires a network of magnetic field measurements and total plasma density images. This information must be sampled on timescales faster than plasma mass is redistributed in order to resolve temporal changes to this distribution (likely minutes or faster). A network of magnetic field measurements over a broad region of space is required to measure fluctuating ULF-wave magnetic fields to establish how ULF wave amplitudes and modes (e.g., field line resonance or propagating mode) are determined by the spatial distribution of total plasma density. The Alfvén speed is also a function of plasma mass density. Therefore, point measurements of ion composition (H^+ , He^+ , and O^+) embedded within the total plasma density image plane are required to determine the extent to which the spatial distribution of cold ions significantly impacts ULF wave properties.

2.6 Objective 3, Science Question 3b: By What Mechanisms and to What Extent Does the Distribution of Plasma Mass Govern the Dynamics of Meso-Scale Plasma Flows That Reach the Inner Magnetosphere?

The Dungey cycle (Dungey, 1961) describes the fundamental flow of magnetic energy and flux through Earth's solar-wind driven magnetosphere. A key portion of the Dungey cycle involves the return flow of magnetic field and plasma sunward from the magnetotail. Numerous studies have established that these return flows take the form of structured plasma flows, often called Bursty Bulk Flows (BBFs) (Baumjohann et al., 1989; Angelopoulos et al., 1992; Angelopoulos et al., 1994; Runov et al., 2011; Wiltberger et al., 2015). The evolution of BBFs is well understood $> \sim 8R_E$ from Earth. BBFs originate in the magnetotail beyond $\sim 15R_E$ (Ohtani et al., 2006; Sitnov et al., 2009; Runov et al., 2011). They are accompanied by dipolarization of the Earth's magnetic field (Angelopoulos, 2008). BBFs are known to be responsible for much of the energy transport from the Earth's magnetotail into the inner magnetosphere [Turner et al. (2015); Stawarz et al. (2016) and references therein] and are known to drive ionospheric energy deposition, as demonstrated by their association with specific auroral forms (Sergeev et al., 1999; Sergeev et al., 2000; Nakamura et al., 2001; Stawarz et al., 2015).

BBF velocities slow to the order of 100 km/s as they travel from $\sim 12R_E$ to $\sim 8R_E$ and the Earth's magnetic field becomes stronger. This region, called the BBF braking region (McPherron et al., 2011), displays strong turbulence, wherein ions and electrons are energized and Alfvén waves are launched toward Earth's ionosphere (Ergun et al., 2015). The fate of BBFs is not well understood Earthward of $\sim 8R_E$, where their flow speed is again dramatically reduced (Reeves et al., 1996; Malaspina et al., 2015).

One of the many unknowns is how BBFs inject energetic particles and heavy ions into the inner magnetosphere (Takada et al., 2006; Dubyagin et al., 2011; Gkioulidou et al., 2014; Turner et al., 2015).

Mounting evidence indicates that the distribution of plasmaspheric mass determines the final deceleration of Earthward plasma flows (Li et al., 2011; Khoo et al., 2018; Glocer et al., 2020; Allison et al., 2021), thereby regulating the deposition of their remaining flow energy into the inner magnetosphere, and their ability to transport plasmasheet particles into the inner magnetosphere (Sorathia et al., 2018). Further, the Poynting flux generated during BBF breaking is implicated in the energization of ions in the ionosphere and subsequent production of low-energy ion outflow that contributes to re-population of the outer plasmasphere (Chaston et al., 2016).

Fundamental aspects of Earthward flow physics cannot be determined using single-point or serendipitous multi-point *in-situ* measurements. A lack of coordinated *in-situ* and context imaging measurements prevents quantitative evaluation of how the energy and mass carried by these flows is redistributed through the inner magnetosphere as they slow and stop. Evidence from multi-spacecraft case studies (Motoba et al., 2020) supports the long-suspected [e.g., Turner et al. (2015) and Turner et al. (2017)] and references therein connection between BBFs and the particle injections that supply the ring current (Gkioulidou et al., 2014), as well as radiation belt source and seed particles (Jaynes et al., 2015).

PILOT achieves closure on this SQ by determining the extent to which cold plasma regulates plasma flow evolution in the inner magnetosphere, including particle injection physics and energy transfer from flows to plasma waves.

A network of magnetic field sensors and rapidly refreshing total density maps are required to end long-persistent questions about the flow spatial structure and deceleration in the inner magnetosphere (e.g., Reeves et al., 1996; Wiltberger et al., 2015; Khoo et al., 2018)). A network of energetic electron flux measurements are required to definitively connect flow deceleration with electron injection spatial and temporal evolution, including energy-dependent radial penetration (Li et al., 2011; Turner et al., 2015; Turner et al., 2017; Khoo et al., 2018; Glocer et al., 2020; Motoba et al., 2020; Allison et al., 2021). Embedded within the density image plane, *in-situ* ground-truth observations are needed. Electron, proton, and heavy ion distribution functions across a wide range of energies (0.1 eV–1 MeV for e- and p+, up to 50 keV for heavy ions) are required to determine the evolution of flow-entrained particles. DC-coupled electric and magnetic field observations are required to definitively identify injection flows. AC-coupled electric and magnetic field measurements are needed to observe dissipation of flow energy into plasma waves. Meridional cold plasma observations, made in concert with the previously described measurements, are needed to constrain the amount of new ion outflow that results from flow-breaking energy input into the ionosphere (Chaston et al., 2016) during the dissipation of flow events. A typical flow is expected to be 1 to $2R_E$ in radial and azimuthal spatial extent, traveling Earthward at 35 km/s with a total plasma density

(n_e) fractional depletion of $\Delta n_e/n_e \approx 50\%$ (Reeves et al., 1996; Runov et al., 2011; Fletcher et al., 2019). Given these parameters, a density image spatial resolution of $\leq 0.5 R_E$ and temporal resolution of < 20 s are needed to fully characterize these flows (Yang et al., 2014; Liu et al., 2015).

2.7 Objective 3, Science Question 3c: To What Extent Does the Dynamic Distribution of Plasma Mass in the Magnetosphere Determine the Expression of Wave-Particle Interactions That Energize, De-Energize, and Precipitate Energetic Plasma?

Plasma waves are a fundamental driver of particle energization and loss in the inner magnetosphere (Horne et al., 2005; Thorne, 2010; Jaynes et al., 2015). Ambient cold plasma density and magnetic field strongly determine the efficiency of the relevant wave-particle interactions on kinetic scales (Young et al., 1981; Kozyra et al., 1984; Summers et al., 1998; Omura et al., 2007). However, our knowledge of the spatial extent of these processes currently relies on an elaborate chain of complex modeling and statistical inference (Ni et al., 2014; Meredith et al., 2018; Zhang et al., 2018; He et al., 2020; Malaspina et al., 2020; Meredith et al., 2020; Delzanno et al., 2021). Predictions resulting from this chain often sharply disagree with any individual geomagnetic event (Jaynes et al., 2018; Watt et al., 2019), especially for extreme driving cases, blurring the picture as to which plasma wave processes are most relevant under which geomagnetic conditions.

Some of the plasma wave modes most effective at sculpting particle populations in the inner magnetosphere are Very Low Frequency (VLF) waves such as chorus and hiss (e.g., Horne et al., 2005; Thorne, 2010; Ripoll et al., 2014; Breneman et al., 2015), and electromagnetic ion cyclotron (EMIC) waves (e.g. Sandanger et al., 2007; Usanova et al., 2014; Shprits et al., 2016).

Plasma density regulates the growth and damping of these wave modes (Nicholson, 1983; Summers et al., 1998; Agapitov et al., 2019). Because of this, the plasmopause defines a sharp boundary between hiss (radiation-belt loss) and chorus (radiation-belt energization and/or loss) (Thorne, 2010; Malaspina et al., 2016; Malaspina et al., 2018), making it a critical boundary for radiation belt dynamics (Baker et al., 2013), auroral precipitation (He et al., 2020) and ionospheric heating (Liang et al., 2018).

The generation and propagation of EMIC waves depend strongly on plasma density and ion composition (Young et al., 1981; Kozyra et al., 1984). In a multi-component plasma, EMIC waves appear frequency bands separated by the cyclotron frequencies of individual ion species. Models show that EMIC source regions overlap with regions of anisotropic ring current protons and plasmaspheric drainage plumes (Jordanova et al., 2001; Chen et al., 2010). Simulated global images of proton precipitation match the temporal and spatial evolution of IMAGE observations of subauroral proton arcs, indicating that cyclotron resonant wave-particle interactions are a viable mechanism for their generation (Jordanova et al., 2007). Observationally, however, the dependence of EMIC waves on cold plasma density and/or density gradients is controversial

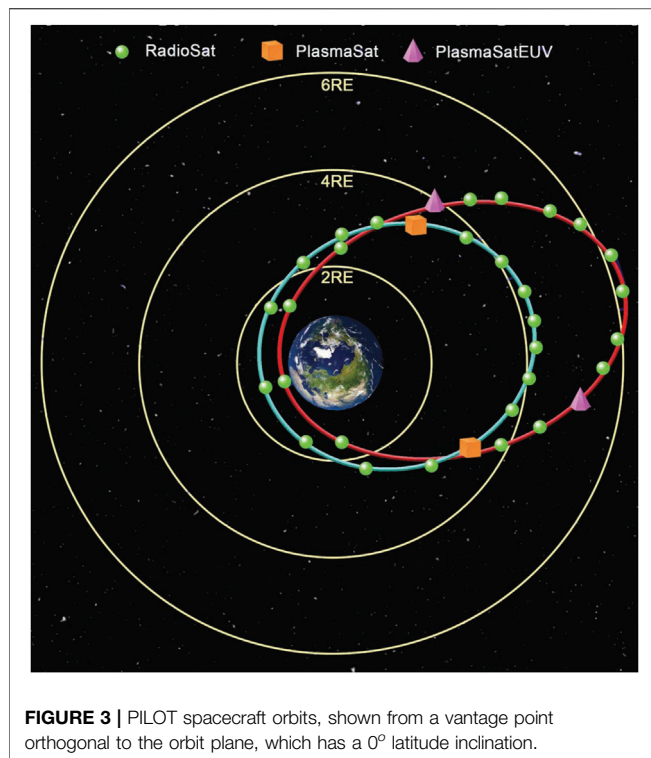


FIGURE 3 | PILOT spacecraft orbits, shown from a vantage point orthogonal to the orbit plane, which has a 0° latitude inclination.

(Usanova et al., 2013; Engebretson et al., 2015; Halford et al., 2015).

PILOT achieves closure on this science question by determining the degree to which the dynamic spatial distribution of cold plasma mass and magnetic field controls the expression (growth, damping) of plasma waves over a broad region of the inner magnetosphere.

A network of magnetic field measurements and rapidly refreshing total plasma density images are required to define the two-dimensional spatial distribution of plasma wave growth conditions near the magnetic equatorial plane. Embedded in this two-dimensional space, *in-situ* measurements of electron, proton, and heavy ion distribution functions, along with AC-coupled electric and magnetic fields, are needed to provide ground-truth point-sampling of energy transfer from particles to plasma waves as the surrounding density and magnetic field conditions that regulate wave properties vary in time and space.

2.8 Science Objectives to Measurements

Figure 2 shows the flow from PILOT's science goal to its science objectives to specific science questions, to targeted physical processes, and finally to required measurements. The required measurements are separated into those made by RadioSats and those made by PlasmaSats. A key maps each measurement number to the physical property being measured.

Cold particles are defined here as having thermal energy between ~ 0.1 and ~ 100 eV. Warm particles are defined from ~ 100 eV to ~ 50 keV, and energetic particles are those with thermal energy from ~ 100 keV to 1 MeV. DC-coupled electric and magnetic fields are defined as fields with fluctuation frequencies between quasi-static

and ~ 20 Hz. AC-coupled fields are defined by frequencies between ~ 10 Hz and 15 kHz for magnetic fields, and between ~ 10 Hz and ~ 500 kHz for electric fields.

The next section describes a mission implementation that is fully capable of making the required PILOT measurements and thereby addressing the PILOT science objectives and questions.

3 MISSION IMPLEMENTATION CONCEPT

3.1 Mission Overview

PILOT uses a constellation of 30 identical microsat spacecraft (RadioSats) and four smallsat spacecraft (PlasmaSats) in two near-equatorial, highly-elliptical orbits. The PILOT orbits are $1.52 R_E \times 4.25 R_E$ and $1.10 R_E \times 6.25 R_E$ (Figure 3). These orbits are chosen to optimize measurements of the most mass-dynamic regions of the inner magnetosphere, particularly near the plasmopause. Over the course of a three-year primary mission, PILOT measures near-equatorial plasma density with images constructed from radio tomography measurements, measures meridional plasma flows with EUV images, and makes embedded *in-situ* fields and particle measurements.

Radio tomography, active plasma sounding, *in-situ* magnetic field, and *in-situ* energetic electron flux measurements are made by 14 RadioSats in the inner orbit and 16 RadioSats in the outer orbit. The RadioSat instrument complement and the heritage of notional instruments is shown in Table 1. RadioSat measurements are complemented by PlasmaSat measurements of DC and AC electric and magnetic fields, as well as proton, ion, and electron distribution functions, as well as local total electron density. These measurements are made by four PlasmaSats, which are identical except that the two PlasmaSats in the outer orbit, PlasmaSatEUVs, also carry EUV cameras that image the spatial distribution and flow of He^+ and O^+ ions in the meridional plane. The PlasmaSat instrument complement and heritage of notional instruments is shown in Table 2.

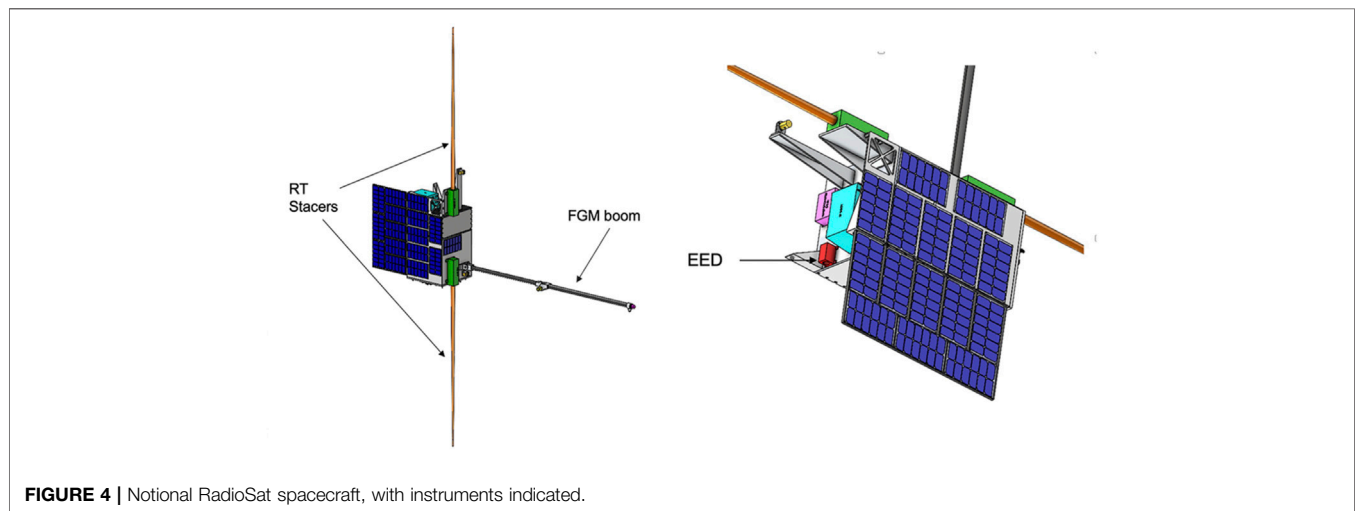
The PILOT flight system design is driven primarily by the orbits required to achieve PILOT science. To maintain the radio tomographic mesh, the two orbits are required to have parallel lines of apsides and precess at the same rate for the full mission duration through all MLTs, and necessarily traverse a high-radiation environment. An orbit design that meets this co-precession requirement uses an inner orbit perigee of $1.52 R_E$. The orbit selected precessed through all MLTs each 1.7 years, allowing 1.75 full precessions through MLT during the nominal 3 year mission. To dispose of the spacecraft on this orbit within 25 years, 40 m/s of delta-V is required to place the inner orbit spacecraft into a graveyard orbit. The outer spacecraft are deorbited into the Earth's atmosphere, requiring 57 m/s of delta-V. The PILOT mission design includes ample propellant to accommodate collision avoidance maneuvers. Parts selection and shielding mass are driven by the requirement to withstand up to 125 krad-Si/year of radiation. The PILOT spacecraft are launched by two Falcon Heavy launch vehicles, one for each orbit, from Cape Canaveral, FL. It should be noted that near-future launch vehicles (for example, the SpaceX Starship), allow the deployment of all PILOT spacecraft in one launch at significantly reduced cost.

TABLE 1 | RadioSat instruments and heritage.

Acronym	Instrument type	Measurement	Heritage
RT	Radio Tomography, relaxation sounder	Total e- content, <i>in-situ</i> e- density	N/A (radio tomography), MAVEN LPW (sounder)
EED	Energetic electron detector	Energetic e- flux	AeroCube10 μ CPT
FGM	Fluxgate Magnetometer	Vector DC magnetic fields	ST-5, GTOsat

TABLE 2 | PlasmaSat instruments and heritage.

Acronym	Instrument type	Measurement	Heritage
EMF FGM	Fluxgate magnetometer	DC magnetic fields	ST-5
EMF SCM	Search coil magnetometer	AC magnetic fields	Van Allen Probes EMFISIS
EMF EFI	Electric field double probes	AC and DC electric fields	Van Allen Probes EFW
EMF APPS	Relaxation sounder	<i>In-situ</i> e- density	MAVEN LPW
PIMS	Ion mass spectrometer	Cold and warm, e ⁻ , p ⁺ , He ⁺ , O ⁺ PADs	Van Allen Probes HOPE
EPS	Energetic particle spectrometer	Energetic e ⁻ /p ⁺ + PADs	GTOsat REMS
EUVCS EUV-He	He ⁺ imager	He ⁺ from 30.4 nm intensity	IMAGE EUV (sensor) JUNO UVS (electronics)
EUVCS EUV-O	O ⁺ /O ⁺⁺ imager	O ⁺ /O ⁺⁺ from 83.4 nm intensity	IMAGE EUV (sensor) JUNO UVS (electronics)

**FIGURE 4** | Notional RadioSat spacecraft, with instruments indicated.

PILOT's mission architecture is resilient to risks associated with the loss of a spacecraft. For example, if up to four RadioSats fail before reaching the baseline mission duration, the remaining RadioSats can be re-positioned to meet the resolution requirement for tomographic imaging with a reduced duty cycle.

3.2 RadioSat

PILOT uses 30 RadioSats: 16 in the inner orbit and 14 in the outer orbit. An industry survey was conducted to determine the capability of current spacecraft providers to produce 30 RadioSats that meet PILOT science and environment requirements. Multiple providers were identified, and the PILOT mission concept adopts a representative RadioSat spacecraft design from this survey.

To facilitate the production of large-quantity RadioSat instruments, PILOT's approach is to have instruments designed by universities or research institutes, but to have instrument manufacture, as well as integration and test completed by commercial companies.

3.2.1 Instrument Payload Description

Each RadioSat carries three scientific instruments: Radio Tomography (RT), Fluxgate Magnetometer (FGM), and Energetic Electron Detector (EED).

The RT instrument consists of two subsystems: Radio Frequency (RF) and Active and Passive Plasma Sounder (APPS), both of which share the same dipole pair of axially-deployed 1.5 m stacer antennas (**Figure 4**) for transmitting and receiving signals. RF transmits dual frequency (50 and 150 MHz) radio signals from each RadioSat to all other RadioSats. The RF on each RadioSat receives these signals and measures their relative phase delay to determine the TEC along the line of sight between spacecraft (Ergun et al., 2000). Two-dimensional total plasma density images are derived from this network of TEC measurements via tomographic inversion. APPS is a relaxation sounder, similar to Cluster Whisper (Trotignon et al., 2003) and the relaxation sounding portion of MAVEN/LPW (Andersson et al., 2015), that measures *in-situ* electron density needed for radio

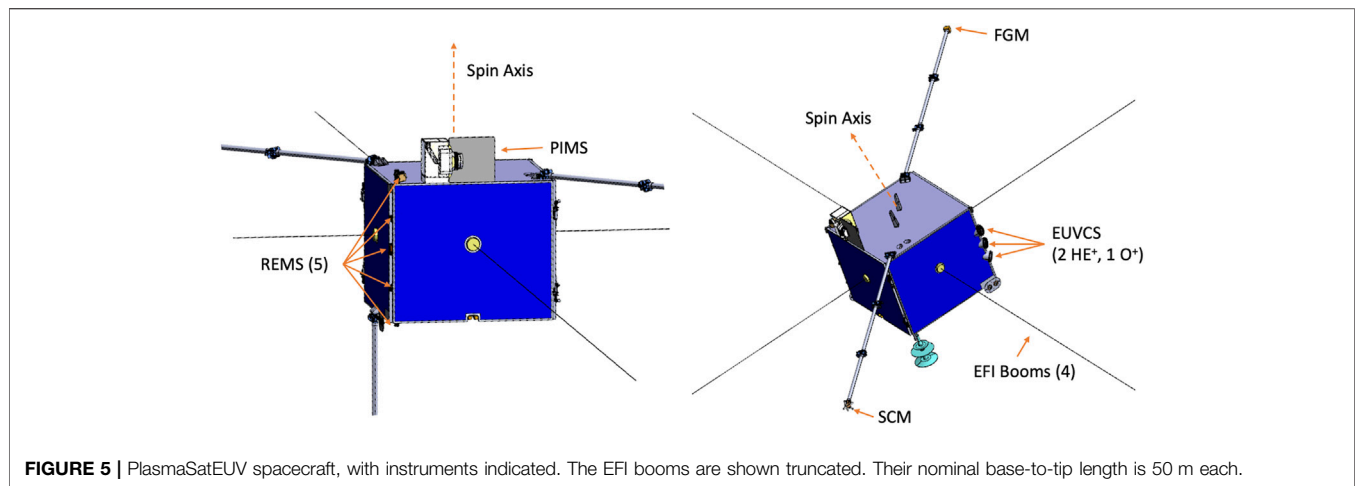


FIGURE 5 | PlasmaSatEUV spacecraft, with instruments indicated. The EFI booms are shown truncated. Their nominal base-to-tip length is 50 m each.

tomographic inversion. APPS stimulates the ambient plasma with a low-power electrostatic signal and measures the frequency of the resultant plasma-resonant waves, both actively and passively. The FGM is located at the end of a 2 m boom and measures the DC-coupled three-axis magnetic field. The network of FGMs measure the detailed terrestrial magnetic field configuration, as well as spatial variation in ULF wave properties. The EED is a compact solid state telescope that measures fluxes of trapped ($\sim 90^\circ$ pitch angle) electrons in the 50 keV–3 MeV range. The science goal of the EED instruments is to resolve time variability of trapped electron fluxes at many locations simultaneously (e.g., observing a front of newly injected electrons pass over each spacecraft in sequence). Therefore, EED does not need to resolve pitch angle, and larger measurement errors compared to non-miniaturized solid-state particle instruments are acceptable for PILOT.

A discussion and demonstration of how RT RF measurements are used to produce images of plasma density for PILOT is presented in **Supplementary Appendix S1**.

3.2.2 Spacecraft

RadioSat spacecraft (**Figure 4**) are three-axis stabilized and carry an X-band high-gain antenna and S-band patch antenna. They contact an Amazon Web Services ground station at each perigee for data downlink and commanding. Their pointing knowledge is determined by combining data from six sun sensors with comparisons between FGM measurements and geomagnetic field models near perigee. Position knowledge is determined via GPS near perigee combined with orbit modeling. Reaction wheels are used for attitude control. RadioSats are deployed on two SpaceX Falcon Heavy launch vehicles, one for each orbit, with four RadioSats mounted per ESPA-Grande port. Once deployed from the launch vehicle, they use on-board propulsion to achieve spacing in mean anomaly to optimize radio tomography image resolution.

3.3 PlasmaSat

PILOT has four PlasmaSat spacecraft. The two on the outer orbit carry EUV imaging instruments (PlasmaSatEUVs), and the two

on the inner orbit do not (PlasmaSats). The PlasmaSat design is driven by the need to spin for particle and fields measurements.

3.3.1 Instrument Payload Description

All four PlasmaSats have identical spacecraft busses, and carry identical copies of the Electromagnetic Fields (EMF) instrument suite, Energetic Particle Sensors (EPS), and the Plasmasphere Ion Mass Spectrometer (PIMS). The two outer-orbit PlasmaSatEUVs also carry an EUV Camera System (EUVCS).

The EMF suite measures *in-situ* electric and magnetic fields across a range of frequencies using several sensors. The Electric Field Instrument (EFI) measures electric fields from DC to ~ 500 kHz along two axes, as well as the spacecraft floating potential, using the double probe technique (Mozer, 2016). A fluxgate magnetometer (FGM) identical to the one flown on the RadioSats, measures the DC-coupled magnetic field vector, and a search coil magnetometer (SCM) measures the AC magnetic field vector. EMF includes identical APPS electronics to the RadioSats. The PlasmaSat APPS uses EFI booms to broadcast and receive relaxation sounding signals. EMF-suite instruments have extensive heritage on magnetospheric missions including the Van Allen Probes (Kletzing et al., 2013; Mauk et al., 2013; Wygant et al., 2013), THEMIS (Angelopoulos, 2008; Bonnell et al., 2008), and MMS (Burch et al., 2015; Torbert et al., 2016).

PIMS obtains *in-situ* distribution functions (flux versus energy, pitch angle, gyrophase angle) and derived moments (density, temperature) for three major ion species (H^+ , He^+ , and O^+) and electrons. PIMS is a nearly identical copy of the Van Allen Probes HOPE instrument that comprises an electrostatic analyzer (ESA) with a time of flight (TOF) subsystem (Funsten et al., 2013). Measurement of full cold ion distributions (down to ~ 0 eV) is enabled by the Sensor-Panel Bias (SPB) system, which applies a voltage to the entire PIMS instrument and its adjacent spacecraft panel relative to the spacecraft chassis ground, allowing cold ions to reach PIMS while minimizing angular deflection.

EPS consists of five electron and proton magnetic spectrometers per PlasmaSat. Together, they measure the *in-situ* distribution functions of energetic electrons (~ 0.2 to ~ 1.5 MeV) and protons (~ 0.15 to ~ 8 MeV). Each spectrometer has a $20^\circ \times 10^\circ$ field of

view, and five spectrometers are arranged on each PlasmaSat such that the 20° portion of their fields of view are symmetrically distributed along the 180° between PlasmaSat spin axes. This arrangement, combined with spacecraft rotation, enables a nearly 4π steradian coverage of the sky. The baseline for the PILOT EPS spectrometer is the REMS instrument on GTOsat (Blum et al., 2020). REMS is a miniaturized version of the MagEIS-Medium instrument on Van Allen Probes (Blake et al., 2013).

EUVCS comprises two imager instruments: EUV-He and EUV-O. EUVCS provides global images of EUV light scattered from He⁺ at 30.4 nm (EUV-He, two cameras) and O⁺/O⁺ at 83.4 nm (EUV-O, one camera). EUVCS images meridional ion distribution, orthogonal and complementary to the equatorial distribution obtained via radio tomography. The optical design shared by EUV-He and EUV-O is an evolution of the IMAGE EUV instrument (Sandel et al., 2000), with an expanded 40° field of view and improved 0.45° resolution (Davis et al., 2013; Goldstein et al., 2022) to image structures as small as 0.05 R_E .

A discussion of inversion and forward modeling algorithms for EUV image deconvolution is given in **Supplementary Appendix S2**.

3.3.2 Spacecraft

PlasmaSat and PlasmaSatEUV spacecraft (**Figure 5**) are identical except for the EUVCS instrument. The bus design is driven by instrument power, mass, and accommodation requirements, the radiation environment, and propellant needed for disposal delta-V. PlasmaSat spacecraft spin at ~5 RPM, and the spin axis is nearly orthogonal to the spacecraft orbital plane. Each PlasmaSat carries a high-gain omnidirectional X-band antenna and contacts Amazon Web Services ground station throughout the orbit to downlink data, and uplink commands once per day. Star trackers are used for attitude determination. Position knowledge is determined using single-way ranging. PlasmaSats are designed with avionics radiation tolerant to 100 krad, and use shielding to provide additional radiation mitigation.

4 CONCLUSION

There are currently large gaps in our understanding of the physical processes that transport mass into, through, and out of the magnetosphere. These processes are fundamental to our understanding of the role that planetary magnetic fields may play in atmospheric retention at terrestrial planets. A comprehensive picture of mass flow dynamics is also critical to understanding how the evolving spatial distribution of magnetospheric plasma mass regulates the behavior of key magnetospheric subsystems, and binds these subsystems together into a coherent whole.

These considerations motivate the primary science goal of PILOT: to determine the primary pathways of mass and energy flow through the coupled systems of the terrestrial magnetosphere. Three science objectives flow from this goal: 1) Identify and quantify the key processes that govern mass and energy exchange between the ionosphere and the magnetosphere, 2) Discover the pathways and processes governing cold plasma mass transport through and out of the inner magnetosphere, and 3) Determine how, where, and when cold plasma mass acts most efficiently to regulate coupling between magnetospheric regions and between plasma populations. To address

these science objectives, the PILOT mission concept ‘follows the mass’ through the magnetosphere, combining simultaneous measurements of the spatial distribution of total plasma density in the near-equatorial plane, the ion density distribution in the meridional plane, and ground-truth *in-situ* measurements of particles and fields.

The PILOT mission implementation concept leverages technological innovations to construct a fully realizable mission from 34 spacecraft: 30 RadioSats that create a radio tomographic mesh for plasma density images, and 4 PlasmaSats carrying comprehensive *in-situ* payloads, with 2 of those 4 also carrying EUV imaging payloads. These 34 spacecraft are arrayed in two co-precessing orbits to provide high spatial and temporal coverage of a large swath of the inner magnetosphere.

The PILOT mission concept is fully capable of making the transformational measurements needed to close fundamental and persistent knowledge gaps about mass and energy flow through the magnetosphere of a magnetized terrestrial planet.

DATA AVAILABILITY STATEMENT

The original contributions presented in the study are included in the article/**Supplementary Material**, further inquiries can be directed to the corresponding author.

AUTHOR CONTRIBUTIONS

All authors supported this mission concept through the development of science objectives, questions and/or instrument or spacecraft implementation. All authors contributed to the text and/or figures included in the manuscript.

FUNDING

Work on the PILOT mission concept was funded by the NASA Heliophysics Mission Concept Studies (HMCS) program *via* award # 80NSSCK0110.

ACKNOWLEDGMENTS

The authors would like to acknowledge helpful discussions and input from the following commercial companies: Aerojet Rocketdyne, The Aerospace Corporation, Amazon Web Services, Ball Aerospace, Blue Canyon Technologies, Blue Origin, Exolaunch GmbH, Microchip Technology Inc., Muon Space, and SpaceX. The companies were not involved in the study design, collection, analysis, interpretation of data, the writing of this article or the decision to submit it for publication.

SUPPLEMENTARY MATERIAL

The Supplementary Material for this article can be found online at: <https://www.frontiersin.org/articles/10.3389/fspas.2022.910730/full#supplementary-material>

REFERENCES

- Agapitov, O., Mourenas, D., Artemyev, A., Hospodarsky, G., and Bonnell, J. W. (2019). Time Scales for Electron Quasi-linear Diffusion by Lower-Band Chorus Waves: The Effects of ω P_e/Q Ce Dependence on Geomagnetic Activity. *Geophys. Res. Lett.* 46, 6178–6187. doi:10.1029/2019GL083446
- Allison, H. J., Shprits, Y. Y., Zhelavskaya, I. S., Wang, D., and Smirnov, A. G. (2021). Gyroresonant Wave-Particle Interactions with Chorus Waves during Extreme Depletions of Plasma Density in the Van Allen Radiation Belts. *Sci. Adv.* 7. doi:10.1126/sciadv.abc0380
- Anderson, P. C., Heelis, R. A., and Hanson, W. B. (1991). The Ionospheric Signatures of Rapid Subauroral Ion Drifts. *J. Geophys. Res.* 96, 5785–5792. doi:10.1029/90ja02651
- Andersson, L., Peterson, W. K., and McBryde, K. M. (2005). Estimates of the Suprathermal O+outflow Characteristic Energy and Relative Location in the Auroral Oval. *Geophys. Res. Lett.* 32, L09104. doi:10.1029/2004GL021434
- Andersson, L., Weber, T. D., Malaspina, D., Crary, F., Ergun, R. E., Delory, G. T., et al. (2015). Dust Observations at Orbital Altitudes Surrounding Mars. *Science* 350, 0398. doi:10.1126/science.aad0398
- Andriopoulou, M., Nakamura, R., Wellenzohn, S., Torkar, K., Baumjohann, W., Torbert, R. B., et al. (2018). Plasma Density Estimates from Spacecraft Potential Using Mms Observations in the Dayside Magnetosphere. *J. Geophys. Res. Space Phys.* 123, 2620–2629. doi:10.1002/2017JA025086
- Angelopoulos, V., Baumjohann, W., Kennel, C. F., Coroniti, F. V., Kivelson, M. G., Pellat, R., et al. (1992). Bursty Bulk Flows in the Inner Central Plasma Sheet. *J. Geophys. Res.* 97, 4027–4039. doi:10.1029/91JA02701
- Angelopoulos, V., Kennel, C. F., Coroniti, F. V., Pellat, R., Kivelson, M. G., Walker, R. J., et al. (1994). Statistical Characteristics of Bursty Bulk Flow Events. *J. Geophys. Res.* 99, 21257–21280. doi:10.1029/94JA01263
- Angelopoulos, V. (2008). The THEMIS Mission. *Space Sci. Rev.* 141, 5–34. doi:10.1007/s11214-008-9336-1
- Baker, D. N., Kanekal, S. G., Hoxie, V. C., Batiste, S., Bolton, M., Li, X., et al. (2013). The Relativistic Electron-Proton Telescope (REPT) Instrument on Board the Radiation Belt Storm Probes (RBSP) Spacecraft: Characterization of Earth's Radiation Belt High-Energy Particle Populations. *Space Sci. Rev.* 179, 337–381. doi:10.1007/s11214-012-9950-9
- Banks, P. M. (1968). Hydrogen Ion Velocity Distributions in the Ionosphere. *Planet. Space Sci.* 16, 759–773. doi:10.1016/0032-0633(68)90080-9
- Banks, P. M. (1969). The Thermal Structure of the Ionosphere. *Proc. IEEE* 57, 258–281. doi:10.1109/proc.1969.6959
- Baumjohann, W., Paschmann, G., and Cattell, C. A. (1989). Average Plasma Properties in the Central Plasma Sheet. *J. Geophys. Res.* 94, 6597–6606. doi:10.1029/JA094iA06p06597
- Bernhardt, P. A., McCoy, R. P., Dymond, K. F., Picone, J. M., Meier, R. R., Kamalabadi, F., et al. (1998). Two-dimensional Mapping of the Plasma Density in the Upper Atmosphere with Computerized Ionospheric Tomography (CIT). *Phys. Plasmas* 5, 2010–2021. doi:10.1063/1.872872
- Blake, J. B., Carranza, P. A., Claudepierre, S. G., Clemmons, J. H., Crain, W. R., Dotan, Y., et al. (2013). The Magnetic Electron Ion Spectrometer (MagEIS) Instruments Aboard the Radiation Belt Storm Probes (RBSP) Spacecraft. *Space Sci. Rev.* 179, 383–421. doi:10.1007/s11214-013-9991-8
- Blum, L. W., Kepko, L., Turner, D., Gabrielse, C., Jaynes, A., Kanekal, S., et al. (2020). “The GTOsat CubeSat: Scientific Objectives and Instrumentation,” in *Micro- and Nanotechnology Sensors, Systems, and Applications XII*. Editors T. George and M. S. Islam (International Society for Optics and Photonics (SPIE)), 62–71. doi:10.1117/12.2556268
- Boardsen, S. A., Gallagher, D. L., Gurnett, D. A., Peterson, W. K., and Green, J. L. (1992). Funnel-shaped, Low-Frequency Equatorial Waves. *J. Geophys. Res.* 97, 14967–14976. doi:10.1029/92JA00827
- Bonnell, J. W., Mozer, F. S., Delory, G. T., Hull, A. J., Ergun, R. E., Cully, C. M., et al. (2008). The Electric Field Instrument (EFI) for THEMIS. *Space Sci. Rev.* 141, 303–341. doi:10.1007/s11214-008-9469-2
- Borovsky, J. E., Denton, M. H., Denton, R. E., Jordanova, V. K., and Krall, J. (2013). Estimating the Effects of Ionospheric Plasma on Solar Wind/magnetosphere Coupling via Mass Loading of Dayside Reconnection: Ion-Plasma-Sheet Oxygen, Plasmaspheric Drainage Plumes, and the Plasma Cloak. *J. Geophys. Res. Space Phys.* 118, 5695–5719. doi:10.1002/jgra.50527
- Borovsky, J. E., Welling, D. T., Thomsen, M. F., and Denton, M. H. (2014). Long-lived Plasmaspheric Drainage Plumes: Where Does the Plasma Come from? *J. Geophys. Res. Space Phys.* 119, 6496–6520. doi:10.1002/2014JA020228
- Breneman, A. W., Halford, A., Millan, R., McCarthy, M., Fennell, J., Sample, J., et al. (2015). Global-scale Coherence Modulation of Radiation-Belt Electron Loss from Plasmaspheric Hiss. *Nature* 523, 193–195. doi:10.1038/nature14515
- Burch, J. L., Mende, S. B., Mitchell, D. G., Moore, T. E., Pollock, C. J., Reinisch, B. W., et al. (2001a). Views of Earth's Magnetosphere with the IMAGE Satellite. *Science* 291, 619–624. doi:10.1126/science.291.5504.619
- Burch, J. L., Mitchell, D. G., Sandel, B. R., Brandt, P. C., and Wüest, M. (2001b). Global Dynamics of the Plasmasphere and Ring Current during Magnetic Storms. *Geophys. Res. Lett.* 28, 1159–1162. doi:10.1029/2000GL012413
- Burch, J. L., Moore, T. E., Torbert, R. B., and Giles, B. L. (2015). Magnetospheric Multiscale Overview and Science Objectives. *Space Sci. Rev.* 199, 5–21. doi:10.1007/s11214-015-0164-9
- Burch, J. L. (2001). The Fury of Space Storms. *Sci. Am.* 284, 86–94. doi:10.1038/scientificamerican0401-86
- Carpenter, D. L., Giles, B. L., Chappell, C. R., Décréau, P. M. E., Anderson, R. R., Persoon, A. M., et al. (1993). Plasmasphere Dynamics in the Dusk-side Bulge Region: A New Look at an Old Topic. *J. Geophys. Res.* 98, 19243–19271. doi:10.1029/93JA00922
- Celnikier, L. M., Harvey, C. C., Jegou, R., Moricet, P., and Kemp, M. (1983). A Determination of the Electron Density Fluctuation Spectrum in the Solar Wind, Using the ISEE Propagation Experiment. *Astronomy Astrophysics* 126, 293–298.
- Chappell, C. R., Huddleston, M. M., Moore, T. E., Giles, B. L., and Delcourt, D. C. (2008). Observations of the Warm Plasma Cloak and an Explanation of its Formation in the Magnetosphere. *J. Geophys. Res.* 113, a–n. doi:10.1029/2007JA012945
- Chappell, C. R. (2015). The Role of the Ionosphere in Providing Plasma to the Terrestrial Magnetosphere - an Historical Overview. *Space Sci. Rev.* 192, 5–25. doi:10.1007/s11214-015-0168-5
- Chaston, C. C., Bonnell, J. W., Reeves, G. D., and Skoug, R. M. (2016). Driving Ionospheric Outflows and Magnetospheric O + Energy Density with Alfvén Waves. *Geophys. Res. Lett.* 43, 4825–4833. doi:10.1002/2016GL069008
- Chen, L., Thorne, R. M., Jordanova, V. K., Wang, C.-P., Gkioulidou, M., Lyons, L., et al. (2010). Global Simulation of EMIC Wave Excitation during the 21 April 2001 Storm from Coupled RCM-RAM-HOTRAY Modeling. *J. Geophys. Res. Space Phys.* 115, A07209. doi:10.1029/2009JA015075
- Claudepierre, S. G., Toffoletto, F. R., and Wiltberger, M. (2016). Global MHD Modeling of Resonant ULF Waves: Simulations with and without a Plasmasphere. *J. Geophys. Res. Space Phys.* 121, 227–244. doi:10.1002/2015JA022048
- Darrouzet, F., Gallagher, D. L., André, N., Carpenter, D. L., Dandouras, I., Décréau, P. M. E., et al. (2009). Plasmaspheric Density Structures and Dynamics: Properties Observed by the Cluster and Image Missions. *Space Sci. Rev.* 145, 55–106. doi:10.1007/s11214-008-9438-9
- Davis, M. W., Gladstone, G. R., Goldstein, J., Sandel, B. R., Greathouse, T. K., Retherford, K. D., et al. (2013). “An Improved Wide-Field Camera for Imaging Earth's Plasmasphere at 30.4 Nm,” in *UV, X-Ray, and Gamma-Ray Space Instrumentation for Astronomy XVIII*. Editor O. H. Siegmund (International Society for Optics and Photonics (SPIE)), 227–235. doi:10.1117/12.2024440
- Delzanno, G. L., Borovsky, J. E., Henderson, M. G., Resendiz Lira, P. A., Roytershteyn, V., and Welling, D. T. (2021). The Impact of Cold Electrons and Cold Ions in Magnetospheric Physics. *J. Atmos. Solar-Terrestrial Phys.* 220, 105599. doi:10.1016/j.jastp.2021.105599
- Dent, Z. C., Mann, I. R., Goldstein, J., Menk, F. W., and Ozeke, L. G. (2006). Plasmaspheric Depletion, Refilling, and Plasmopause Dynamics: A Coordinated Ground-Based and IMAGE Satellite Study. *J. Geophys. Res.* 111, A03205. doi:10.1029/2005JA011046
- Denton, M. H., and Borovsky, J. E. (2014). Observations and Modeling of Magnetic Flux Tube Refilling of the Plasmasphere at Geosynchronous Orbit. *J. Geophys. Res. Space Phys.* 119, 9246–9255. doi:10.1002/2014ja020491
- Denton, R. E., Goldstein, J., Lee, D.-H., King, R. A., Dent, Z. C., Gallagher, D. L., et al. (2006). Realistic Magnetospheric Density Model for 29 August 2000. *J. Atmos. Solar-Terrestrial Phys.* 68, 615–628. doi:10.1016/j.jastp.2005.11.009
- Denton, R. E., Wang, Y., Webb, P. A., Tengdin, P. M., Goldstein, J., Redfern, J. A., et al. (2012). Magnetospheric electron density long-term (> 1 day) refilling rates inferred from passive radio emissions measured by IMAGE RPI during

- geomagnetically quiet times. *J. Geophys. Res.* 117, a–n. doi:10.1029/2011JA017274
- Dubyagin, S., Sergeev, V., Apatenkov, S., Angelopoulos, V., Runov, A., Nakamura, R., et al. (2011). Can Flow Bursts Penetrate into the Inner Magnetosphere? *Geophys. Res. Lett.* 38, a–n. doi:10.1029/2011GL047016
- Dungey, J. W. (1955). Electrodynamics of the Outer Atmosphere. *Phys. Ionos.* 229.
- Dungey, J. W. (1961). Interplanetary Magnetic Field and the Auroral Zones. *Phys. Rev. Lett.* 6, 47–48. doi:10.1103/PhysRevLett.6.47
- Elkington, S. R., Hudson, M. K., and Chan, A. A. (2003). Resonant Acceleration and Diffusion of Outer Zone Electrons in an Asymmetric Geomagnetic Field. *J. Geophys. Res.* 108, 1116. doi:10.1029/2001JA009202
- Elphic, R. C., Thomsen, M. F., and Borovsky, J. E. (1997). The Fate of the Outer Plasmasphere. *Geophys. Res. Lett.* 24, 365–368. doi:10.1029/97GL00141
- Engebretson, M. J., Posch, J. L., Wygant, J. R., Kletzing, C. A., Lessard, M. R., Huang, C. L., et al. (2015). Van Allen Probes, NOAA, GOES, and Ground Observations of an Intense EMIC Wave Event Extending over 12 H in Magnetic Local Time. *J. Geophys. Res. Space Phys.* 120, 5465–5488. doi:10.1002/2015JA021227
- Engwall, E., Eriksson, A. I., Cully, C. M., André, M., Torbert, R., and Vaith, H. (2009). Earth's Ionospheric Outflow Dominated by Hidden Cold Plasma. *Nat. Geosci.* 2, 24–27. doi:10.1038/ngeo387
- Ergun, R. E., Goodrich, K. A., Stawarz, J. E., Andersson, L., and Angelopoulos, V. (2015). Large-amplitude Electric Fields Associated with Bursty Bulk Flow Braking in the Earth's Plasma Sheet. *J. Geophys. Res. Space Phys.* 120, 1832–1844. doi:10.1002/2014JA020165
- Ergun, R. E., Larson, D. E., Phan, T., Taylor, D., Bale, S., Carlson, C. W., et al. (2000). Feasibility of a Multisatellite Investigation of the Earth's Magnetosphere with Radio Tomography. *J. Geophys. Res.* 105, 361–373. doi:10.1029/1999JA900170
- Farrugia, C. J., Young, D. T., Geiss, J., and Balsiger, H. (1989). The Composition, Temperature, and Density Structure of Cold Ions in the Quiet Terrestrial Plasmasphere: GEOS 1 Results. *J. Geophys. Res.* 94, 11865–11891. doi:10.1029/JA094iA09p11865
- Fletcher, A. C., Crabtree, C., Ganguli, G., Malaspina, D., Tejero, E., and Chu, X. (2019). Kinetic Equilibrium and Stability Analysis of Dipolarization Fronts. *J. Geophys. Res. Space Phys.* 124, 2010–2028. doi:10.1029/2018JA026433
- Foster, J. C., Erickson, P. J., Walsh, B. M., Wygant, J. R., Coster, A. J., and Zhang, Q. H. (2020). *Multi-Point Observations of the Geospace Plume*. American Geophysical Union, 243–264. chap. 14. doi:10.1002/9781119509592.ch14
- Foster, J. C., Rideout, W., Sandel, B., Forrester, W. T., and Rich, F. J. (2007). On the Relationship of Saps to Storm-Enhanced Density. *J. Atmos. Solar-Terrestrial Phys.* 69, 303–313. doi:10.1016/j.jastp.2006.07.021
- Funsten, H. O., Skoug, R. M., Guthrie, A. A., MacDonald, E. A., Baldonado, J. R., Harper, R. W., et al. (2013). Helium, Oxygen, Proton, and Electron (HOPE) Mass Spectrometer for the Radiation Belt Storm Probes Mission. *Space Sci. Rev.* 179, 423–484. doi:10.1007/s11214-013-9968-7
- Gallagher, D. L., and Adrian, M. L. (2007). Two-dimensional Drift Velocities from the IMAGE EUV Plasmaspheric Imager. *J. Atmos. Solar-Terrestrial Phys.* 69, 341–350. doi:10.1016/j.jastp.2006.05.028
- Gallagher, D. L., Comfort, R. H., Katus, R. M., Sandel, B. R., Fung, S. F., and Adrian, M. L. (2021). The Breathing Plasmasphere: Erosion and Refilling. *J. Geophys. Res. Space Phys.* 126, e2020JA028727. doi:10.1029/2020JA028727
- Gallagher, D. L., and Comfort, R. H. (2016). Unsolved Problems in Plasmasphere Refilling. *J. Geophys. Res. Space Phys.* 121, 1447–1451. doi:10.1002/2015ja022279
- Galvan, D. A., Moldwin, M. B., Sandel, B. R., and Crowley, G. (2010). On the Causes of Plasmaspheric Rotation Variability: IMAGE EUV Observations. *J. Geophys. Res. (Space Phys.)* 115, A01214. doi:10.1029/2009JA014321
- Gkioulidou, M., Ukhorskiy, A. Y., Mitchell, D. G., Sotiropoulos, T., Mauk, B. H., and Lanzerotti, L. J. (2014). The Role of Small-Scale Ion Injections in the Buildup of Earth's Ring Current Pressure: Van Allen Probes Observations of the 17 March 2013 Storm. *J. Geophys. Res. Space Phys.* 119, 7327–7342. doi:10.1002/2014JA020096
- Glocer, A., Welling, D., Chappell, C. R., Toth, G., Fok, M.-C., Komar, C., et al. (2020). A Case Study on the Origin of Near-Earth Plasma. *J. Geophys. Res. Space Phys.* 125, e2020JA028205. doi:10.1029/2020JA028205
- Goldstein, J., Chappell, C. R., Davis, M. W., Denton, M. H., Denton, R. E., Gallagher, D. L., et al. (2018). Imaging the Global Distribution of Plasmaspheric Oxygen. *J. Geophys. Res. Space Phys.* 123, 2078–2103. doi:10.1002/2017JA024531
- Goldstein, J., Gallagher, D., Craven, P. D., Comfort, R. H., Genestreti, K. J., Mouikis, C., et al. (2019). Temperature Dependence of Plasmaspheric Ion Composition. *J. Geophys. Res. Space Phys.* 124, 6585–6595. doi:10.1029/2019JA026822
- Goldstein, J., Gallagher, D. L., Molyneux, P., and Reeves, G. D. (2021). “Core-Plasma Refilling and Erosion: Science Justification,” in *Heliophysics 2050 White Papers (NASA Heliophysics Division) (MAGNETOSPHERE SCIENCE, #4063)*.
- Goldstein, J., Gallagher, D. L., Sandel, B. R., Davis, M., Molyneux, P., Veach, T., et al. (2020). “The Future of Plasmaspheric Extreme Ultraviolet (EUV) Imaging,” in *Magnetospheric Imaging (Elsevier)*, 231. Chapter 6. doi:10.1016/B978-0-12-820630-0.00010-6
- Goldstein, J., Gallagher, D. L., Sandel, B. R., Davis, M., Molyneux, P., Veach, T., et al. (2022). “The Future of Plasmaspheric Extreme Ultraviolet (EUV) Imaging,” in *Understanding the Space Environment through Global Measurements*. Editors Y. Colado-Vega, D. Gallagher, H. Frey, and S. Wing (Elsevier), 231–286. doi:10.1016/B978-0-12-820630-0.00010-6
- Goldstein, J., and Sandel, B. R. (2005). The Global Pattern of Evolution of Plasmaspheric Drainage Plumes. *Wash. D.C. Am. Geophys. Union Geophys. Monogr. Ser.* 159, 1–22. doi:10.1029/159gm02
- Goldstein, J., Sandel, B. R., Thomsen, M. F., Spasojević, M., and Reiff, P. H. (2004a). Electric Fields Deduced from Plasmopause Motion in IMAGE EUV Images. *Geophysical Research Letters* 31 (1), L01801–22. doi:10.1029/2003GL018797
- Goldstein, J., Spasojević, M., Reiff, P. H., Sandel, B. R., Forrester, W. T., Gallagher, D. L., et al. (2003). Identifying the Plasmopause in IMAGE EUV Data Using IMAGE RPI *In Situ* Steep Density Gradients. *J. Geophys. Res.* 108, 1147. doi:10.1029/2002JA009475
- Goldstein, J., Wolf, R. A., Sandel, B. R., and Reiff, P. H. (2004b). Electric Fields Deduced from Plasmopause Motion in IMAGE EUV Images. *Geophys. Res. Lett.* 31, L01801. doi:10.1029/2003GL018797
- Gurnett, D. A. (1976). Plasma Wave Interactions with Energetic Ions Near the Magnetic Equator. *J. Geophys. Res.* 81, 2765–2770. doi:10.1029/JA081i016p02765
- Halford, A. J., Fraser, B. J., and Morley, S. K. (2015). EMIC Waves and Plasmaspheric and Plume Density: CRRES Results. *J. Geophys. Res. Space Phys.* 120, 1974–1992. doi:10.1002/2014JA020338
- He, F., Guo, R.-L., Dunn, W. R., Yao, Z.-H., Zhang, H.-S., Hao, Y.-X., et al. (2020). Plasmopause Surface Wave Oscillates the Magnetosphere and Diffuse Aurora. *Nat. Commun.* 11, 1668. doi:10.1038/s41467-020-15506-3
- Hill, S., Buzulukova, N., Boardsen, S., and Fok, M.-C. (2020). Local Heating of Oxygen Ions in the Presence of Magnetosonic Waves: Possible Source for the Warm Plasma Cloak? *J. Geophys. Res. Space Phys.* 125, e2019JA027210. doi:10.1029/2019ja027210
- Horne, R. B., Thorne, R. M., Shprits, Y. Y., Meredith, N. P., Glauert, S. A., Smith, A. J., et al. (2005). Wave Acceleration of Electrons in the Van Allen Radiation Belts. *Nature* 437, 227–230. doi:10.1038/nature03939
- Horwitz, J. L., and Lockwood, M. (1985). The Cleft Ion Fountain: A Two-Dimensional Kinetic Model. *J. Geophys. Res.* 90, 9749. doi:10.1029/JA090iA10p09749
- Hrbáčková, Z., Santolík, O., Němec, F., Macušíková, E., and Cornilleau-Wehrlin, N. (2015). Systematic Analysis of Occurrence of Equatorial Noise Emissions Using 10 Years of Data from the Cluster Mission. *J. Geophys. Res. Space Phys.* 120, 1007–1021. doi:10.1002/2014JA020268
- Hull, A. J., Chaston, C. C., Bonnell, J. W., Wygant, J. R., Kletzing, C. A., Reeves, G. D., et al. (2019). Dispersive Alfvén Wave Control of O⁺ Ion Outflow and Energy Densities in the Inner Magnetosphere. *Geophys. Res. Lett.* 46. doi:10.1002/2019GL083808.1029/2019gl083808
- Hultqvist, B., Øieroset, M., Paschmann, G., and Treumann, R. A. (1999). *Magnetospheric Plasma Sources and Losses*. Springer. doi:10.1007/978-94-011-4477-3
- Jahn, J.-M., Goldstein, J., Reeves, G. D., Fernandes, P. A., Skoug, R. M., Larsen, B. A., et al. (2017). The Warm Plasma Composition in the Inner Magnetosphere during 2012–2015. *J. Geophys. Res. Space Phys.* 122, 11–018. doi:10.1002/2017ja024183
- Jakosky, B. M. (2015). MAVEN Explores the Martian Upper Atmosphere. *Science* 350, 643. doi:10.1126/science.aad3443

- Jaynes, A. N., Ali, A. F., Elkington, S. R., Malaspina, D. M., Baker, D. N., Li, X., et al. (2018). Fast Diffusion of Ultrarelativistic Electrons in the Outer Radiation Belt: 17 March 2015 Storm Event. *Geophys. Res. Lett.* 45, 10,874–10,882. doi:10.1029/2018GL079786
- Jaynes, A. N., Baker, D. N., Singer, H. J., Rodriguez, J. V., Loto'aniu, T. M., Ali, A. F., et al. (2015). Source and Seed Populations for Relativistic Electrons: Their Roles in Radiation Belt Changes. *J. Geophys. Res. Space Phys.* 120, 7240–7254. doi:10.1002/2015JA021234
- Jordanova, V. K., Farrugia, C. J., Thorne, R. M., Khazanov, G. V., Reeves, G. D., and Thomsen, M. F. (2001). Modeling Ring Current Proton Precipitation by Electromagnetic Ion Cyclotron Waves during the May 14–16, 1997, Storm. *J. Geophys. Res.* 106, 7–22. doi:10.1029/2000JA002008
- Jordanova, V. K., Spasojevic, M., and Thomsen, M. F. (2007). Modeling the Electromagnetic Ion Cyclotron Wave-Induced Formation of Detached Subauroral Proton Arcs. *J. Geophys. Res.* 112, a–n. doi:10.1029/2006JA012215
- Khoo, L. Y., Li, X., Zhao, H., Sarris, T. E., Xiang, Z., Zhang, K., et al. (2018). On the Initial Enhancement of Energetic Electrons and the Innermost Plasmapause Locations: Coronal Mass Ejection-Driven Storm Periods. *J. Geophys. Res. Space Phys.* 123, 9252–9264. doi:10.1029/2018JA026074
- Kivelson, M. G., and Southwood, D. J. (1985). Resonant ULF Waves: A New Interpretation. *Geophys. Res. Lett.* 12, 49–52. doi:10.1029/GL0121001p00049
- Kletzing, C. A., Kurth, W. S., Acuna, M., MacDowall, R. J., Torbert, R. B., Averkamp, T., et al. (2013). The Electric and Magnetic Field Instrument Suite and Integrated Science (EMFISIS) on RBSP. *Space Sci. Rev.* 179, 127–181. doi:10.1007/s11214-013-9993-6
- Kozyra, J. U., Cravens, T. E., Nagy, A. F., Fontheim, E. G., and Ong, R. S. B. (1984). Effects of Energetic Heavy Ions on Electromagnetic Ion Cyclotron Wave Generation in the Plasmapause Region. *J. Geophys. Res.* 89, 2217–2234. doi:10.1029/JA089iA04p02217
- Krall, J., Huba, J. D., and Borovsky, J. E. (2018). Sami3 Simulations of a Persistent Plasmasphere Plume. *Geophys. Res. Lett.* 45, 3374–3381. doi:10.1002/2017gl076448
- Kunduri, B. S. R., Baker, J. B. H., Ruohoniemi, J. M., Nishitani, N., Oksavik, K., Erickson, P. J., et al. (2018). A New Empirical Model of the Subauroral Polarization Stream. *J. Geophys. Res. Space Phys.* 123, 7342–7357. doi:10.1029/2018JA025690
- Kurth, W. S., De Pascuale, S., Faden, J. B., Kletzing, C. A., Hospodarsky, G. B., Thaller, S., et al. (2015). Electron Densities Inferred from Plasma Wave Spectra Obtained by the Waves Instrument on Van Allen Probes. *J. Geophys. Res. Space Phys.* 120, 904–914. doi:10.1002/2014JA020857
- Lawrence, D. J., Thomsen, M. F., Borovsky, J. E., McComas, D. J., and McComas, D. J. (1999). Measurements of Early and Late Time Plasmasphere Refilling as Observed from Geosynchronous Orbit. *J. Geophys. Res.* 104, 14691–14704. doi:10.1029/1998JA900087
- Lee, D.-H., and Lysak, R. L. (1989). Magnetospheric ULF Wave Coupling in the Dipole Model: The Impulsive Excitation. *J. Geophys. Res.* 94, 17097–17103. doi:10.1029/JA094iA12p17097
- Leitinger, R., Ladreiter, H.-P., and Kirchengast, G. (1997). Ionosphere Tomography with Data from Satellite Reception of Global Navigation Satellite System Signals and Ground Reception of Navy Navigation Satellite System Signals. *Radio Sci.* 32, 1657–1669. doi:10.1029/97RS01027
- Lemaire, J. F., Gringauz, K. I., Carpenter, D. L., and Bassolo, V. (1998). *The Earth's Plasmasphere*. Cambridge: Cambridge University Press. doi:10.1017/CBO9780511600098
- Li, S. S., Angelopoulos, V., Runov, A., Zhou, X. Z., McFadden, J., Larson, D., et al. (2011). On the Force Balance Around Dipolarization Fronts within Bursty Bulk Flows. *J. Geophys. Res. (Space Phys.)* 116, A00I35. doi:10.1029/2010JA015884
- Liang, J., Donovan, E., Reimer, A., Hampton, D., Zou, S., and Varney, R. (2018). Ionospheric Electron Heating Associated with Pulsating Auroras: Joint Optical and Pfirs Observations. *J. Geophys. Res. Space Phys.* 123, 4430–4456. doi:10.1029/2017JA025138
- Liemohn, M. W., Ridley, A. J., Gallagher, D. L., Ober, D. M., and Kozyra, J. U. (2004). Dependence of Plasmaspheric Morphology on the Electric Field Description during the Recovery Phase of the 17 April 2002 Magnetic Storm. *J. Geophys. Res.* 109, A03209. doi:10.1029/2003JA010304
- Liu, J., Angelopoulos, V., Zhou, X.-Z., Yao, Z.-H., and Runov, A. (2015). Cross-tail Expansion of Dipolarizing Flux Bundles. *J. Geophys. Res. Space Phys.* 120, 2516–2530. doi:10.1002/2015JA020997
- Lysak, R. L. (1990). Electrodynamic Coupling of the Magnetosphere and Ionosphere. *Space Sci. Rev.* 52, 33–87. doi:10.1007/BF00704239
- Malaspina, D. M., Jaynes, A. N., Boulé, C., Bortnik, J., Thaller, S. A., Ergun, R. E., et al. (2016). The Distribution of Plasmaspheric Hiss Wave Power with Respect to Plasmapause Location. *Geophys. Res. Lett.* 43, 7878–7886. doi:10.1002/2016GL069982
- Malaspina, D. M., Ripoll, J. F., Chu, X., Hospodarsky, G., and Wygant, J. (2018). Variation in Plasmaspheric Hiss Wave Power with Plasma Density. *Geophys. Res. Lett.* 45, 9417–9426. doi:10.1029/2018GL078564
- Malaspina, D. M., Zhu, H., and Drozdov, A. Y. (2020). A Wave Model and Diffusion Coefficients for Plasmaspheric Hiss Parameterized by Plasmapause Location. *J. Geophys. Res. (Space Phys.)* 125, e27415. doi:10.1029/2019JA027415
- Malaspina, D., Wygant, J., Ergun, R., Reeves, G., Skoug, R., and Larsen, B. (2015). Electric Field Structures and Waves at Plasma Boundaries in the Inner Magnetosphere. *J. Geophys. Res. (Space Phys.)* 120. doi:10.1002/2015JA021137
- Maruyama, N., Sun, Y. Y., Richards, P. G., Middlecoff, J., Fang, T. W., Fuller-Rowell, T. J., et al. (2016). A New Source of the Midlatitude Ionospheric Peak Density Structure Revealed by a New Ionosphere-Plasmasphere Model. *Geophys. Res. Lett.* 43, 2429–2435. doi:10.1002/2015GL067312
- Matsui, H., Torbert, R. B., Spence, H. E., Khotyaintsev, Y. V., and Lindqvist, P.-A. (2013). Revision of Empirical Electric Field Modeling in the Inner Magnetosphere Using Cluster Data. *J. Geophys. Res. Space Phys.* 118, 4119–4134. doi:10.1002/jgra.50373
- Mauk, B. H., Fox, N. J., Kanekal, S. G., Kessel, R. L., Sibeck, D. G., and Ukhorskiy, A. (2013). Science Objectives and Rationale for the Radiation Belt Storm Probes Mission. *Space Sci. Rev.* 179, 3–27. doi:10.1007/s11214-012-9908-y
- McPherron, R. L., Hsu, T.-S., Kissinger, J., Chu, X., and Angelopoulos, V. (2011). Characteristics of Plasma Flows at the Inner Edge of the Plasma Sheet. *J. Geophys. Res. (Space Phys.)* 116, A00I33. doi:10.1029/2010JA015923
- Meier, R. R., Nicholas, A. C., Picone, J. M., Melendez-Alvira, D. J., Ganguli, G. I., Reynolds, M. A., et al. (1998). Inversion of Plasmaspheric EUV Remote Sensing Data from the STP 72-1 Satellite. *J. Geophys. Res.* 103, 17505–17518. doi:10.1029/98JA011175
- Meredith, N. P., Horne, R. B., Kersten, T., Li, W., Bortnik, J., Sicard, A., et al. (2018). Global Model of Plasmaspheric Hiss from Multiple Satellite Observations. *J. Geophys. Res. Space Phys.* 123, 4526–4541. doi:10.1029/2018JA025226
- Meredith, N. P., Horne, R. B., Shen, X.-C., Li, W., and Bortnik, J. (2020). Global Model of Whistler Mode Chorus in the Near-Equatorial Region ($-\lambda_m - i 18^\circ$). *Geophys. Res. Lett.* 47, e87311. doi:10.1029/2020GL087311
- Morton, Y. J., Yang, Z., Breitsch, B., Bourne, H., and Rino, C. (2020). *Ionospheric Effects, Monitoring, and Mitigation Techniques*. John Wiley & Sons, 879–937. chap. 31. doi:10.1002/9781119458449.ch31
- Motoba, T., Ohtani, S., Claudepierre, S. G., Reeves, G. D., Ukhorskiy, A. Y., and Lanzerotti, L. J. (2020). Dynamic Properties of Particle Injections inside Geosynchronous Orbit: A Multisatellite Case Study. *J. Geophys. Res. Space Phys.* 125, e2020JA028215. doi:10.1029/2020JA028215
- Mozer, F. S. (2016). DC and Low-Frequency Double Probe Electric Field Measurements in Space. *J. Geophys. Res. (Space Phys.)* 121, 10,942–10,953. doi:10.1002/2016JA022952
- Nakamura, R., Baumjohann, W., Schödel, R., Brittnacher, M., Sergeev, V. A., Kubysheva, M., et al. (2001). Earthward Flow Bursts, Auroral Streamers, and Small Expansions. *J. Geophys. Res.* 106, 10791–10802. doi:10.1029/2000JA000306
- Nakano, S., Fok, M.-C., Brandt, P. C., and Higuchi, T. (2014a). Estimation of Temporal Evolution of the Helium Plasmasphere Based on a Sequence of IMAGE/EUV Images. *J. Geophys. Res. Space Phys.* 119, 3708–3723. doi:10.1002/2013JA019734
- Nakano, S., Fok, M.-C., Brandt, P. C., and Higuchi, T. (2014b). Estimation of the Helium Ion Density Distribution in the Plasmasphere Based on a Single IMAGE/EUV Image. *J. Geophys. Res. Space Phys.* 119, 3724–3740. doi:10.1002/2013JA019733
- Nass, H. U., and Fahr, H. J. (1984). Plasma-gas Interactions in Planetary Atmospheres and Their Relevance for the Terrestrial Hydrogen Budget. *J. Geophys. Zeitschrift Geophys.* 56, 34–46.
- Ni, B., Li, W., Thorne, R. M., Bortnik, J., Ma, Q., Chen, L., et al. (2014). Resonant Scattering of Energetic Electrons by Unusual Low-Frequency Hiss. *Geophys. Res. Lett.* 41, 1854–1861. doi:10.1002/2014GL059389

- Nicholson, D. R. (1983). *Introduction to Plasma Theory*. New York: John Wiley & Sons.
- Nosé, M., Matsuoka, A., Kumamoto, A., Kasahara, Y., Goldstein, J., Teramoto, M., et al. (2018). Longitudinal Structure of Oxygen Torus in the Inner Magnetosphere: Simultaneous Observations by Arase and Van Allen Probe A. *Geophys. Res. Lett.* 45. doi:10.1002/2018GL080122. doi:10.1002/2018gl080122
- Nosé, M., Oimatsu, S., Keika, K., Kletzing, C. A., Kurth, W. S., Pascuale, S. D., et al. (2015). Formation of the Oxygen Torus in the Inner Magnetosphere: Van Allen Probes Observations. *J. Geophys. Res. Space Phys.* 120, 1182–1196. doi:10.1002/2014ja020593
- Nosé, M., Oimatsu, S., Keika, K., Kletzing, C. A., Kurth, W. S., Pascuale, S. D., et al. (2015). Formation of the Oxygen Torus in the Inner Magnetosphere: Van Allen Probes Observations. *J. Geophys. Res. Space Phys.* 120, 1182–1196. doi:10.1002/2014JA020593
- Nosé, M., Takahashi, K., Anderson, R. R., and Singer, H. J. (2011). Oxygen Torus in the Deep Inner Magnetosphere and its Contribution to Recurrent Process of O⁺-rich Ring Current Formation. *J. Geophys. Res.* 116, a–n. doi:10.1029/2011JA016651
- Ohtani, S., Singer, H. J., and Mukai, T. (2006). Effects of the Fast Plasma Sheet Flow on the Geosynchronous Magnetic Configuration: Geotail and GOES Coordinated Study. *J. Geophys. Res.* 111, A01204. doi:10.1029/2005JA011383
- Olsen, R. C., Shawhan, S. D., Gallagher, D. L., Green, J. L., Chappell, C. R., and Anderson, R. R. (1987). Plasma Observations at the Earth's Magnetic Equator. *J. Geophys. Res.* 92, 2385–2407. doi:10.1029/JA092iA03p02385
- Omura, Y., Furuya, N., and Summers, D. (2007). Relativistic Turning Acceleration of Resonant Electrons by Coherent Whistler Mode Waves in a Dipole Magnetic Field. *J. Geophys. Res. (Space Phys.)* 112, A06236. doi:10.1029/2006JA012243
- Park, C. G. (1974). Some Features of Plasma Distribution in the Plasmasphere Deduced from Antarctic Whistlers. *J. Geophys. Res.* 79, 169–173. doi:10.1029/JA079i001p00169
- Park, C. G. (1973). Whistler Observations of the Depletion of the Plasmasphere during a Magnetospheric Substorm. *J. Geophys. Res.* 78, 672–683. doi:10.1029/JA078i004p00672
- Pierrard, V., and Lemaire, J. (2004). Development of Shoulders and Plumes in the Frame of the Interchange Instability Mechanism for Plasmapause Formation. *Geophys. Res. Lett.* 31. doi:10.1029/2003gl018919
- Ramstad, R., and Barabash, S. (2021). Do Intrinsic Magnetic Fields Protect Planetary Atmospheres from Stellar Winds? *Space Sci. Rev.* 217, 36. doi:10.1007/s11214-021-00791-1
- Reeves, G. D., Henderson, M. G., McLachlan, P. S., Belian, R. D., Friedel, R. H. W., and Korth, A. (1996). “Radial Propagation of Substorm Injections,” in International Conference on Substorms, Vol. 389. ESA Special Publication. Editors E. J. Rolfe and B. Kaldeich (Paris: European Space Agency), 579.
- Reinisch, B. W., Huang, X., Song, P., Green, J. L., Fung, S. F., Vasyliunas, V. M., et al. (2004). Plasmaspheric Mass Loss and Refilling as a Result of a Magnetic Storm. *J. Geophys. Res.* 109, A01202. doi:10.1029/2003JA009948
- Ripoll, J.-F., Albert, J. M., and Cunningham, G. S. (2014). Electron Lifetimes from Narrowband Wave-Particle Interactions within the Plasmasphere. *J. Geophys. Res. Space Phys.* 119, 8858–8880. doi:10.1002/2014JA020217
- Roberts, W. T., Horwitz, J. L., Comfort, R. H., Chappell, C. R., Waite, J. H., and Green, J. L. (1987). Heavy Ion Density Enhancements in the Outer Plasmasphere. *J. Geophys. Res.* 92, 13499. doi:10.1029/JA092iA12p13499
- Roelof, E. C., Mauk, B. H., and Meier, R. R. (1992). “Instrument Requirements for Imaging the Magnetosphere in Extreme Ultraviolet and Energetic Neutral Atoms Derived from Computer-Simulated Images,” in Instrumentation for Magnetospheric Imagery, Vol. 1744 of Society of Photo-Optical Instrumentation Engineers (SPIE) Conference Series. Editor S. Chakrabarti (SPIE), 19–30. doi:10.1117/12.60576
- Runov, A., Angelopoulos, V., Zhou, X.-Z., Zhang, X.-J., Li, S., Plaschke, F., et al. (2011). A THEMIS Multicase Study of Dipolarization Fronts in the Magnetotail Plasma Sheet. *J. Geophys. Res.* 116, A05216. doi:10.1029/2010JA016316
- Samson, J. C., Harrold, B. G., Ruohoniemi, J. M., Greenwald, R. A., and Walker, A. D. M. (1992). Field Line Resonances Associated with MHD Waveguides in the Magnetosphere. *Geophys. Res. Lett.* 19, 441–444. doi:10.1029/92GL00116
- Samson, J. C., and Rostoker, G. (1972). Latitude-dependent Characteristics of High-Latitude Pc 4 and Pc 5 Micropulsations. *J. Geophys. Res.* 77, 6133–6144. doi:10.1029/JA077i031p06133
- Sandanger, M., Soraas, F., Aarsnes, K., Oksavik, K., and Evans, D. S. (2007). Loss of Relativistic Electrons: Evidence for Pitch Angle Scattering by Electromagnetic Ion Cyclotron Waves Excited by Unstable Ring Current Protons. *J. Geophys. Res. (Space Phys.)* 112, A12213. doi:10.1029/2006JA012138
- Sandel, B. R., Broadfoot, A. L., Curtis, C. C., King, R. A., Stone, T. C., Hill, R. H., et al. (2000). The Extreme Ultraviolet Imager Investigation for the IMAGE Mission. *Space Sci. Rev.* 91, 197–242. doi:10.1023/A:1005263510820
- Sandel, B. R. (2011). Composition of the Plasmasphere and Implications for Refilling. *Geophys. Res. Lett.* 38, a–n. doi:10.1029/2011GL048022
- Sandel, B. R., and Denton, M. H. (2007). Global View of Refilling of the Plasmasphere. *Geophys. Res. Lett.* 34, L17102. doi:10.1029/2007GL030669
- Sandel, B. R., King, R. A., Forrester, W. T., Gallagher, D. L., Broadfoot, A. L., and Curtis, C. C. (2001). Initial Results from the IMAGE Extreme Ultraviolet Imager. *Geophys. Res. Lett.* 28, 1439–1442. doi:10.1029/2001GL012885
- Sergeev, V. A., Liou, K., Meng, C.-I., Newell, P. T., Brittnacher, M., Parks, G., et al. (1999). Development of Auroral Streamers in Association with Localized Impulsive Injections to the Inner Magnetotail. *Geophys. Res. Lett.* 26, 417–420. doi:10.1029/1998GL900311
- Sergeev, V. A., Sauvaud, J.-A., Popescu, D., Kovrazhkin, R. A., Liou, K., Newell, P. T., et al. (2000). Multiple-spacecraft Observation of a Narrow Transient Plasma Jet in the Earth's Plasma Sheet. *Geophys. Res. Lett.* 27, 851–854. doi:10.1029/1999GL010729
- Shprits, Y. Y., Drozdov, A. Y., Spasojevic, M., Kellerman, A. C., Usanova, M. E., Engebretson, M. J., et al. (2016). Wave-induced Loss of Ultra-relativistic Electrons in the Van Allen Radiation Belts. *Nat. Commun.* 7, 12883. doi:10.1038/ncomms12883
- Singh, N. (1996). Effects of Electrostatic Ion Cyclotron Wave Instability on Plasma Flow during Early Stage Plasmaspheric Refilling. *J. Geophys. Res.* 101, 17217–17227. doi:10.1029/96JA01008
- Singh, N., and Horwitz, J. L. (1992). Plasmasphere Refilling: Recent Observations and Modeling. *J. Geophys. Res.* 97, 1049. doi:10.1029/91JA02602
- Sitnov, M. I., Swisdak, M., and Divin, A. V. (2009). Dipolarization Fronts as a Signature of Transient Reconnection in the Magnetotail. *J. Geophys. Res.* 114, a–n. doi:10.1029/2008JA013980
- Sojka, J. J., Rasmussen, C. E., and Schunk, R. W. (1986). An Interplanetary Magnetic Field Dependent Model of the Ionospheric Convection Electric Field. *J. Geophys. Res.* 91, 11281–11290. doi:10.1029/JA091iA10p11281
- Sorathia, K. A., Ukhorskiy, A. Y., Merkin, V. G., Fennell, J. F., and Claudepierre, S. G. (2018). Modeling the Depletion and Recovery of the Outer Radiation Belt during a Geomagnetic Storm: Combined MHD and Test Particle Simulations. *J. Geophys. Res. Space Phys.* 123, 5590–5609. doi:10.1029/2018JA025506
- Stawarz, J. E., Ergun, R. E., and Goodrich, K. A. (2015). Generation of High-Frequency Electric Field Activity by Turbulence in the Earth's Magnetotail. *J. Geophys. Res. Space Phys.* 120, 1845–1866. doi:10.1002/2014JA020166
- Stawarz, J. E., Eriksson, S., Wilder, F. D., Ergun, R. E., Schwartz, S. J., Pouquet, A., et al. (2016). Observations of Turbulence in a Kelvin-Helmholtz Event on 8 September 2015 by the Magnetospheric Multiscale Mission. *J. Geophys. Res. Space Phys.* 121, 11,021–11,034. doi:10.1002/2016JA023458
- Summers, D., Thorne, R. M., and Xiao, F. (1998). Relativistic Theory of Wave-Particle Resonant Diffusion with Application to Electron Acceleration in the Magnetosphere. *J. Geophys. Res.* 103, 20487–20500. doi:10.1029/98JA01740
- Takada, T., Nakamura, R., Baumjohann, W., Asano, Y., Volwerk, M., Zhang, T. L., et al. (2006). Do BBFs Contribute to Inner Magnetosphere Dipolarizations: Concurrent Cluster and Double Star Observations. *Geophys. Res. Lett.* 33, L21109. doi:10.1029/2006GL027440
- Takahashi, K., Denton, R. E., Kurth, W., Kletzing, C., Wygant, J., Bonnell, J., et al. (2015). Externally Driven Plasmaspheric ULF Waves Observed by the Van Allen Probes. *J. Geophys. Res. Space Phys.* 120, 526–552. doi:10.1002/2014JA020373
- Thorne, R. M. (2010). Radiation Belt Dynamics: The Importance of Wave-Particle Interactions. *Geophys. Res. Lett.* 37, a–n. doi:10.1029/2010GL044990
- Titov, D. V., Svedhem, H., McCoy, D., Lebreton, J.-P., Barabash, S., Bertaux, J.-L., et al. (2006). Venus Express: Scientific Goals, Instrumentation, and Scenario of the Mission. *Cosm. Res.* 44, 334–348. doi:10.1134/S0010952506040071
- Torbert, R. B., Russell, C. T., Magnes, W., Ergun, R. E., Lindqvist, P.-A., LeContel, O., et al. (2016). The FIELDS Instrument Suite on MMS: Scientific Objectives, Measurements, and Data Products. *Space Sci. Rev.* 199, 105–135. doi:10.1007/s11214-014-0109-8

- Trotignon, J. G., Décréau, P. M. E., Rauch, J. L., Le Guirriec, E., Canu, P., and Darrouzet, F. (2003). The Whisper Relaxation Sounder Onboard Cluster: A Powerful Tool for Space Plasma Diagnosis Around the Earth. *Cosmic Res.* 41, 345–348. doi:10.1023/a:1025045308666
- Turner, D. L., Claudepierre, S. G., Fennell, J. F., O'Brien, T. P., Blake, J. B., Lemon, C., et al. (2015). Energetic Electron Injections Deep into the Inner Magnetosphere Associated with Substorm Activity. *Geophys. Res. Lett.* 42, 2079–2087. doi:10.1002/2015GL063225
- Turner, D. L., Fennell, J. F., Blake, J. B., Claudepierre, S. G., Clemmons, J. H., Jaynes, A. N., et al. (2017). Multipoint Observations of Energetic Particle Injections and Substorm Activity during a Conjunction between Magnetospheric Multiscale (MMS) and Van Allen Probes. *J. Geophys. Res. Space Phys.* 122, 11,481–11,504. doi:10.1002/2017JA024554
- Usanova, M. E., Darrouzet, F., Mann, I. R., and Bortnik, J. (2013). Statistical Analysis of EMIC Waves in Plasmaspheric Plumets from Cluster Observations. *J. Geophys. Res. Space Phys.* 118, 4946–4951. doi:10.1002/jgra.50464
- Usanova, M. E., Drozdov, A., Orlova, K., Mann, I. R., Shprits, Y., Robertson, M. T., et al. (2014). Effect of EMIC Waves on Relativistic and Ultrarelativistic Electron Populations: Ground-Based and Van Allen Probes Observations. *Geophys. Res. Lett.* 41, 1375–1381. doi:10.1002/2013GL059024
- Watt, C. E. J., Allison, H. J., Meredith, N. P., Thompson, R. L., Bentley, S. N., Rae, I. J., et al. (2019). Variability of Quasilinear Diffusion Coefficients for Plasmaspheric Hiss. *J. Geophys. Res. Space Phys.* 124, 8488–8506. doi:10.1029/2018JA026401
- Welling, D. T., André, M., Dandouras, I., Delcourt, D., Fazakerley, A., Fontaine, D., et al. (2015). The Earth: Plasma Sources, Losses, and Transport Processes. *Space Sci. Rev.* 192, 145–208. doi:10.1007/s11214-015-0187-2
- Wiltberger, M., Merkin, V., Lyon, J. G., and Ohtani, S. (2015). High-resolution Global Magnetohydrodynamic Simulation of Bursty Bulk Flows. *J. Geophys. Res. Space Phys.* 120, 4555–4566. doi:10.1002/2015ja021080
- Wright, A. N. (1996). Transfer of Magnetosheath Momentum and Energy to the Ionosphere along Open Field Lines. *J. Geophys. Res.* 101, 13169–13178. doi:10.1029/96JA00541
- Wygant, J. R., Bonnell, J. W., Goetz, K., Ergun, R. E., Mozer, F. S., Bale, S. D., et al. (2013). The Electric Field and Waves Instruments on the Radiation Belt Storm Probes Mission. *Space Sci. Rev.* 179, 183–220. doi:10.1007/s11214-013-0013-7
- Yang, J., Toffoletto, F. R., and Wolf, R. A. (2014). RCM-E Simulation of a Thin Arc Preceded by a North-South-Aligned Auroral Streamer. *Geophys. Res. Lett.* 41, 2695–2701. doi:10.1002/2014GL059840
- Young, D. T., Perraut, S., Roux, A., de Villedary, C., Gendrin, R., Korth, A., et al. (1981). Wave-particle Interactions Near Ω_{He^+} Observed in GEOS 1 and 2. 1. Propagation of Ion Cyclotron Waves in He⁺-rich Plasma. *J. Geophys. Res.* 86, 6755–6772. doi:10.1029/JA086iA08p06755
- Zhang, W., Fu, S., Gu, X., Ni, B., Xiang, Z., Summers, D., et al. (2018). Electron Scattering by Plasmaspheric Hiss in a Nightside Plume. *Geophys. Res. Lett.* 45, 4618–4627. doi:10.1029/2018GL077212

Conflict of Interest: Authors LD and JP are employed by Advanced Space LLC.

The remaining authors declare that the research was conducted in the absence of any commercial or financial relationships that could be construed as a potential conflict of interest.

Publisher's Note: All claims expressed in this article are solely those of the authors and do not necessarily represent those of their affiliated organizations, or those of the publisher, the editors, and the reviewers. Any product that may be evaluated in this article, or claim that may be made by its manufacturer, is not guaranteed or endorsed by the publisher.

Copyright © 2022 Malaspina, Ergun, Goldstein, Spittler, Andersson, Borovsky, Chu, De Moudt, Gallagher, Jordanova, Lejosne, Link, Maruyama, Parker, Thaller, Unruh and Walsh. This is an open-access article distributed under the terms of the Creative Commons Attribution License (CC BY). The use, distribution or reproduction in other forums is permitted, provided the original author(s) and the copyright owner(s) are credited and that the original publication in this journal is cited, in accordance with accepted academic practice. No use, distribution or reproduction is permitted which does not comply with these terms.